別紙１

厚生労働科学研究費補助金

創薬基盤推進研究事業

肉腫および悪性中皮腫を標的破壊する腫瘍溶解性ウイルスベクターのシードストックおよび臨床ロットの製造とその安全性・有効性評価に関する研究

平成１９年度　総括研究報告書

主任研究者　高橋　克仁

別紙２

目　　次

別紙3・4

厚生労働科学研究費補助金(ヒトゲノム・再生医療等研究事業)
(総括・分担)研究報告書
肉腫および悪性中皮腫を標的破壊する腫瘍溶解性ウイルスベクターの
シードストックおよび臨床ロットの製造とその安全性・有効性評価に関する研究
主任研究者　高橋　克仁　大阪府立成人病センター部長

研究要旨　難治性肉腫と悪性中皮腫の治療法開発への国民の要請は極めて強い。申請者らは、遺伝子組換え技術を用いて肉腫と悪性中皮腫を標的破壊する腫瘍溶解性単純ヘルペスウイルスベクターを開発した。本研究では、国内ワクチンメーカーの技術協力の下、わが国初の無菌環境下閉鎖系セル・ベクタープロセシングアイソレーターを用いて、上記ウイルスの精製方法の確立・効力試験・生物学的評価試験を実施し、臨床試験に使用可能なウイルスシードストックを製造する。

分担研究者氏名・所属機関名及び所属機関における職名
山村倫子・大阪府立成人病センター
主任研究員
川口　寧・東京大学
準教授
城野洋一郎・化学及び血清療法研究所
次長
菅原敬信・化学及び血清療法研究所
次長

A. 研究目的
平滑筋肉腫など難治性肉腫と悪性中皮腫に対する腫瘍溶解性単純ヘルペスウイルスを用いた標的遺伝子療法の速やかかつ適切な実用化・臨床応用を目指し、1)遺伝子治療剤*d*12.CALPΔRRおよび*d*12.ODDΔRRのバルクハーベスト、ウイルスシードストック、臨床試験に使用可能なバルク精製標品をセルベクタープロセシングアイソレーターで製造し、2)平滑筋肉腫と悪性中皮腫を対象にした効力試験および生物学的評価試験を実施する。

B. 研究方法
1)　単純ヘルペスウイルスのα遺伝子群に属する転写因子であるICP4を恒常的に発現するVero細胞のデザイナーセルを用いて、カルポニンプロモーターでICP4の合成を制御するカルポニン標的化組換えHSV-1　*d*12.CALPΔRRを無血清培地で増殖させ、精製法を確立する(平成18年度)。
2) ヒト悪性中皮腫に対するin vivoでの抗腫瘍効果のさらなる検討を行うため、効力試験の評価実験系を確立する(平成18年度)。
3) 低酸素応答配列でICP4の分解を制御し固形腫瘍全般を標的化し得る組換えHSV-1 *d*12.ODDΔRRの効力試験(平成19年度)。
4) ウイルスのバルクハーベスト、ウイルスシードストック、バルク精製標品をGMP基準を満たす施設、設備のもとで精製する方法を確立する(平成19年度)。
4) ウイルスのバルクハーベストおよびバルク精製標品の生物学的評価試験、非臨床試験を実施する(平成19、20年度)。

(倫理面への配慮)
検体の採取にあたっては本研究目的で新たに書面による同意が得られた試料のみを使用する。患者検体の解析にあたっては、個人情報の保護に細心の注意を払い、試料、検体、標本は、施錠可能な冷凍庫、キャビネットに保管する。匿名化システムを用いて連結可能匿名化する。検査や解析のため外部機関に提供する場合は暗号化する。試験期間終了後の保管・管理について被験者の同意が得られた検体は主任研究者の所属部門で保管管理する。将来本研究以外の目的に使用する場合は、改めて被験者から使用について同意を得るものとする。

C. 結果
平成19年度は、研究方法の項3)に関して、ヒト平滑筋肉腫と悪性中皮腫培養細胞をSCIDマウスの背部皮下に移植した実験系と平成18年度に確立したヒト腹膜悪性中皮腫培養細胞にルシフェラーゼ標識遺伝子を導入し、SCIDマウス腹腔内に移植するオルソトピックなマウス実験モデルを用いて、*d*12.ODDΔRRの効力試験を実施した。1 x 10^3 pfuのウイルスを腫瘍内または腹腔内に3日間隔で7回直接注入する方法で、強力かつ持続的な抗腫瘍効果を得た。特に*d*12.ODDΔRRがカルポニン非発現腫瘍にも治療効果をもつことを確認した。また、安定なウイルスゲノムDNAの増幅と塩基配列決定のため、BACmidへのクローニングベクターを作成した。方法の項4)に関し、ウイルスバルクハーベストからアフィニティー担体を用いてウイルスシードストックを精製する簡便かつ迅速な新規精製方法を確立した。さらに方法の項5)に関し、生物学的評価試験に使用する抗HSV-1抗体を作成した。

D. 考察
1)固形腫瘍全般を標的化し得る組換えHSV-1 d12.ODDΔRRは、低酸素条件にある細胞において選択的にICP4蛋白が産生される。一方ヒト悪性中皮腫では低酸素によって誘導される種々の遺伝子が発現しており、腫瘍細胞の内部環境が低酸素状態にあると推測されている。d12.ODDΔRRの効力試験の結果は、d12.ODDΔRRがウイルスの力価でみれば、悪性中皮腫治療薬としてこれまでのどのウイルス治療薬よりも優れていることを示している。
2)ウイルスゲノムのBACmidへの挿入は、ゲノムの安定性に寄与し、これまでの課題であったウイルス遺伝子治療薬の規格を均一化するのに役立つものと思われる。
3)抗HSV-1抗体を作成したことにより、平成20年度に計画されている、ウイルスのバルクハーベストおよびバルク精製標品の生物学的評価試験、非臨床試験に向け準備が整った。

E. 結論
1)研究代表者らが我が国で独自に開発したカルポニンプロモーターでICP4の合成を制御するカルポニン標的化組換えHSV-1 d12.CALPΔRRと低酸素応答配列でICP4の分解を制御し固形腫瘍全般を標的化し得る組換えHSV-1 d12.ODDΔRRのヒト悪性中皮腫に対する有効性をマウスの実験モデルで確認した。
2)ウイルスバルクハーベストからアフィニティー担体を用いてウイルスシードストックを精製する簡便かつ迅速な新規精製方法を確立した。
生物学的評価試験に使用する抗HSV-1抗体を作製した。。

F. 健康危険情報
(該当しない)

G. 研究発表
1. 論文発表
Yamamura, H. Takahashi K.et al.
Loss of smooth muscle calponin results in impaired blood vessel maturation in the tumor-host microenvironment. Cancer Sci. 98, 757-763 2007
Iwahori,S., Shirata N., Kawaguchi Y et al., Enhanced Phosphorylation of Transcription Factor Sp1 dependent on Ataxia Telangiectasia -Mutated (ATM) in response to Herpes Simplex Virus Type I Infection. J. Virol. 81: 9653-9664, 2007.
Asai R., Kawaguchi Y. et al. Identification of proteins directly phosphorylated by UL13 protein kinase from herpes simplex virus 1. Microbes and Infection 9: 1434-1438, 2007.
Abe M, Kino Y. et al. Duration of neutralizing antibody titer after Japanese encephalitis vaccination. Microbiol Immunol. 51(6):609-616, 2007

2. 学会発表
高橋克仁、山村倫子 癌幹細胞のマーカーであるCD133が消化管間質腫瘍(GIST)において強く発現していた
第66回日本癌学会学術総会(於横浜)
10月3－5日、2007年
山村倫子、高橋克仁、強力な悪性中皮腫治療薬としてのカルポニン標的化腫瘍溶解性HSV-1の新しい変種
第66回日本癌学会学術総会
(於横浜)10月3－5日、2007年
高橋克仁、山村倫子 ウイルス工学を応用したがん細胞標的医薬の開発;肉腫・中皮腫・がん幹細胞の標的化
第45回日本癌治療学会学術総会(於京都)
シンポジウム9月20日、2007年

Takahashi K, Yamamura H. GIST stem cells
5th Kuningas Foundation GIST Symposium (Helsinki, Finland), January 18-19, 2008
Yamamura H., Takahashi K. Robust CD133 expression and stem cell features of gastro-intestinal stromal tumors (GIST). 13th Annual CTOS Meeting, (Seatle, U.S.A.), November 1-3, 2007

H. 知的財産権の出願・登録状況
(予定を含む。)
1. 特許取得
「ヘルペスウイルス精製法」
高橋克仁、山村倫子(出願予定)

別紙5

発表者氏名	論文タイトル名	発表誌名	巻号	ページ	出版年
Yamamura, H. Hirano, N. Koyama, H., Nishizawa, Y., Takahashi K.	Loss of smooth muscle calponin results in impaired blood vessel maturation in the tumor-host microenvironment.	Cancer Sci.	98	757-763	2007
Iwahori, S. Shirata, N Kawaguchi, Y Weller, S.K. Sato,Y. Kudoh, A. Nakayama, S. Isomura, H. Tsurumi. T.	Enhanced Phosphorylation of Transcription Factor Sp1 dependent on Ataxia Telangiectasia-Mutated (ATM) in response to Herpes Simplex Virus Type I Infection.	J. Virol.	81	9653-9664	2007
Asai, R. Ohno, T. Kato, A. Kawaguchi, Y.	Identification of proteins directly phosphorylated by UL13 protein kinase from herpes simplex virus 1.	Microbes and Infection	9	1434-1438	2007
Abe M, Okada K, Hayashida K, Matsuo F, Shiosaki K, Miyazaki C, Ueda K, Kino Y.	Duration of neutralizing antibody titer after Japanese encephalitis vaccination.	Microbiol Immunol.	51	609-616	2007

Loss of smooth muscle calponin results in impaired blood vessel maturation in the tumor–host microenvironment

Hisako Yamamura,[1] Noriko Hirano,[1] Hidenori Koyama,[2] Yoshiki Nishizawa[2] and Katsuhito Takahashi[1,3]

[1]Department of Molecular Medicine and Pathophysiology, Osaka Medical Center for Cancer and Cardiovascular Diseases, Graduate School of Pharmaceutical Science, Osaka University, Osaka City, Osaka 537-8511; [2]Department of Metabolism, Endocrinology, and Molecular Medicine, Osaka City University Graduate School of Medicine, Osaka City, Osaka 545-8585, Japan

(Received November 26, 2006/Revised December 25, 2006/Accepted December 26, 2006/Online publication March 19, 2007)

The interactions between malignant cells and the microenvironment of the local host tissue play a critical role in tumor growth, metastasis and their response to treatment modalities. We investigated the roles of smooth muscle calponin (*Cnn1*, also called calponin h1 or basic calponin) in the development of tumor vasculature *in vivo* by analyzing mutant mice lacking the *Cnn1* gene. Here we show that loss of *Cnn1* in host mural cells prevents maturation of tumor vasculature. *In vitro* studies showed that platelet-derived growth factor B-induced vascular smooth muscle migration was downregulated by the *Cnn1*-deficiency, and forced expression of *Cnn1* restored migration. Moreover, destruction of established tumor mass by treatment with an antivascular endothelial growth factor antibody was markedly enhanced in *Cnn1*-deficient mice. These data, coupled with the knowledge that structural fragility of normal blood vessels is caused by loss of the *Cnn1* gene, suggest that *Cnn1* plays an important role in the maturation of blood vessels, and may have implications for therapeutic strategies targeting tumor vasculature for treatment of human cancers. (*Cancer Sci* 2007; 98: 757–763)

Smooth muscle calponin (*Cnn1*) is an actin-associated protein originally isolated from vascular smooth muscle,[1] and is a major regulator of force production in smooth muscle cells (SMC).[2–4] It is generally agreed that *Cnn1* expression serves as an excellent marker for defining lineage specification, differentiation and phenotypic modulation of SMC.[5–7] In previous studies on human cancers, we and others have reported positive and negative expression of *Cnn1* in the mural SMC of tumor vasculature,[8–10] and showed that reduced expression of *Cnn1* in the tumor vasculature of patients with the early stage of hepatocellular carcinoma,[8] and those with renal cell carcinoma,[10] was statistically correlated with poor prognosis. Furthermore, a 17-gene signature set was identified in the tumor–host microenvironment to predict metastatic potential and early death for a variety of human solid tumors.[11] These include decreased expression of the smooth muscle genes γ2 actin (*Actg2*), myosin heavy chain 11 (*MYH11*) and *Cnn1*. However, as yet there is no explanation for links between tumor phenotypes and the observed downregulation of the *Cnn1* gene in host cells, including vascular cells. Although a critical role of the calponin gene in the development of normal vasculature has recently been reported in zebrafish,[12] the role of *Cnn1* in the development and maturation of mammalian blood vessels, especially the tumor vasculature, has not been studied.

Materials and Methods

Cells, animals and antibodies. Lewis lung carcinoma cell line (LLC) was purchased from Riken Cell Bank (RCB0558; Tsukuba, Japan). B16 melanoma cells with low metastatic activity to the lung were kindly provided by Dr H. Tanaka (Osaka Medical Center, Osaka, Japan). *Cnn1*-deficient mice,[13] with a genetic background of C57BL6/J (*Cnn1*$^{-/-}$), were generated through back-crossing to C57BL6/J mice (Nihon SLC, Hamamatsu, Japan) for more than 15 generations. Immunoblot analysis was carried out as described previously.[13] Animal procedures were approved by the Animal Care and Use Committee of Osaka Medical Center.

Antibodies and immunohistochemistry. A polyclonal antibody specific to the *Cnn1* isoform was prepared as described previously.[13] Anti-smooth muscle α-actin (α-SMA) (clone 1A4) was purchased from Sigma Chemicals (St Louis, MO, USA). Anti-PECAM-1(CD31) (clone MEC13.3) was from BD PharMingen (San Diego, CA, USA). Anti-PDGFRβ (sc-6252, A-3) was from Santa Cruz Biotechnology (Santa Cruz, CA, USA). Anti-mouse CD34 (clone MEC14.7) was from Hycult Biotechnology (Uden, the Netherland). Anti-NG2 was from Chemicon International (Temacula, CA, USA).

The specimens were fixed in Bouin's solution (15% [v/v] saturated picric acid solution, 1.65% [v/v] formalin and 1% [v/v] acetic acid/phosphate-buffered saline [PBS]) or 10% formaldehyde/PBS and embedded in paraffin. Antigen retrieval was carried out using an autoclave at 121°C for 10 min in a 10-mM citrate buffer (pH 7.0) (*Cnn1*, α-SMA, CD34 and NG2). The procedures described previously[8,13] are available from the authors on request. For staining of CD31, excised tumor specimens were mounted in OCT compound (Miles, Elkhart, USA) and then frozen using liquid nitrogen.

Quantification of the vasculature. Individual microvessel counts, as revealed by CD31 or CD34 expression in the endothelium, were carried out using ×400 fields by two independent investigators after assessing for uniformity of staining at low-power fields (×100). Vessel density is expressed as the number of vessel profiles per mm^2. In accordance with other published studies,[14,15] the fraction of blood vessels found to be associated with α-SMA-positive cells in more than 50% of the vessel perimeter was defined as the pericyte coverage index. The extent of pericyte coverage on vessels was determined on 15 properly cross-sectioned vessels in each specimen by measuring the proportion of CD31- or CD34-positive vessel perimeter covered by α-SMA-immunoreactive cells. Thirty fields per section and at least two tissue sections were counted.

Diffusion chamber model of angiogenesis. LLC cells (4×10^7/mL cells in 200 μL of serum-free Dulbecco's modified Eagle's medium [DMEM]) were injected into the diffusion chamber ring (PR00-014-00; Millipore, Bedford, MA, USA), and the

[3]To whom correspondence should be addressed.
E-mail: takahasi-ka@mc.pref.osaka.jp
The authors declare that they have no competing financial interests.

doi: 10.1111/j.1349-7006.2007.00452.x

chamber was inserted into the skin fold on the back of 6-week-old BALB/c athymic nude mice. Tissues containing angiogenic vasculature were excised 6 days after the implantation, fixed in Bouin's solution, sectioned and immunostained with the anti-*Cnn1* antibody.

Preparation of primary cultured vascular smooth muscle cells. Aortas from 4-week-old wild-type and *Cnn1*$^{-/-}$ mice were minced and incubated for 2 h at 37°C in 1.0 mg/mL collagenase (Worthington Biochemicals, Lakewood, NJ, USA), 0.375 mg/mL soybean trypsin inhibitor (Worthington Biochemicals), 0.125 mg/mL elastase III (Sigma Chemicals) and 2 mg/mL bovine serum albumin (BSA) in HEPES buffer (pH 7.5). Cells were washed, cultured in DMEM containing 10% FCS and characterized by spindle-shaped morphology and immunostaining for α-SMA.

Migration assay and construction of adenovirus vectors. Migration was assayed in a 48-well chamber (Nucleopore, Bethesda, MD, USA) with a polycarbonate filter (PVP free, 8 μm pores) coated with 300 μg/mL type I collagen. SMC (1×10^4 per well) were added to the top wells of the chamber in DMEM containing 0.25% BSA. The bottom wells were filled with DMEM containing 10 ng/mL recombinant platelet-derived growth factor (PDGF)-B/B (Gibco BRL, Carlsbad, CA, USA). The chambers were then incubated for 4 h at 37°C in a humidified atmosphere with 5% CO_2. The filters were fixed and stained with Diff-Quik (Kokusai Shiyaku, Kobe, Japan), and migrated cells were counted. Recombinant adenovirus (Ad) vectors expressing *Escherichia coli LacZ* or human *Cnn1* were generated using unique *I-CeuI* and *PI-SceI* sites in the E1 deletion region.[16] Ad-*Cnn1* and Ad-*LacZ* were prepared by transfection to human embryonic kidney 293 cells.

***In vivo* treatment of vascular endothelial growth factor (VEGF)-neutralizing antibody.** LLC cells (1×10^7/mL in 50 μL PBS) were injected subcutaneously into 6-week-old male wild-type and *Cnn1*$^{-/-}$ mice ($n = 8$ each), and tumor size was monitored. At 10 days after injection, the 'VEGF ablation' groups ($n = 4$) were treated with 8 μg per mouse of goat antimouse VEGF-neutralizing antibody (AF-493-NA; R&D Systems, Minneapolis, MN, USA) administered intraperitoneally every 72 h. Control groups ($n = 4$) were treated with 8 μg per mouse of non-immune goat IgG. Treatment was stopped after a total of four injections.

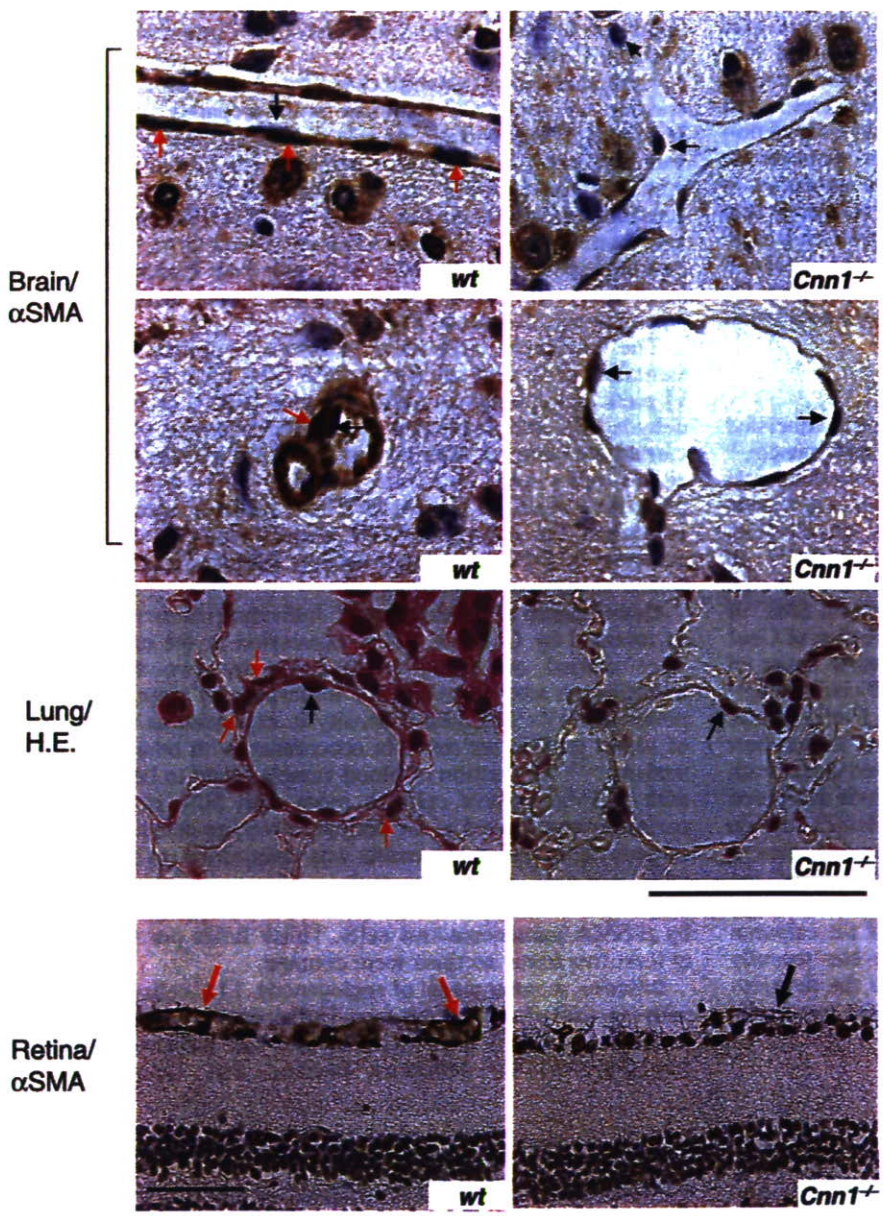

Fig. 1. Impaired maturation of blood vessels in normal tissues in smooth muscle calponin-deficient (*Cnn1*)$^{-/-}$ mice. Capillaries in brain (smooth muscle α-actin [α-SMA] immunostaining), lung (hematoxylin–eosin [H&E] staining) and retina (α-SMA immunostaining) in *Cnn1*$^{-/-}$ mice showed loss of pericytes/smooth muscle cells (SMC) (red arrows) attachment to the endothelium (black arrows). Note the dilation of the *Cnn1*$^{-/-}$ capillary in brain. Scale bar = 50 μm in brain and lung, or 100 μm in retina.

doi: 10.1111/j.1349-7006.2007.00452.x

***In situ* apoptosis detection.** Apoptosis was detected by the modified terminal deoxynucleotidyl transferase-mediated deoxyuridine triphosphate-biotin nick-end labeling (TUNEL) method, using an *In Situ* Apoptosis Detection Kit (Takara Biomedicals, Tokyo, Japan) according to the manufacturer's methods.

Statistical analysis. Statistical differences were determined using the unpaired Student's *t*-test. Differences were considered statistically significant at $P < 0.05$.

Results and Discussion

Microvessels in the brain cortex, lung sections and retina from 6-week-old *Cnn1*$^{-/-}$ mice were found to have thinner walls with fewer mural cell layers than those from wild-type mice. Enlarged and naked endothelial tubes were scored in 16/132 cases in wild-type brain sections ($n = 3$) and in 166/218 cases in *Cnn1*$^{-/-}$ brain sections ($n = 5$). Representative examples from the α-SMA- or hematoxylin–eosin (H&E) staining of the brain, lung and retina sections are shown in Fig. 1. Reduced numbers of α-SMA-positive mural cells in *Cnn1*$^{-/-}$ mice were demonstrated in the immunohistochemistry of the brain and retina sections (Fig. 1). These findings are reminiscent of the impaired recruitment of pericytes to brain capillaries in mice lacking PDGF-B[17] or PDGF receptor (R)-β,[18] and are consistent with ultrastructural studies on the microvessels in the ocular fundus, lung and heart of *Cnn1*$^{-/-}$ mice, demonstrating reduced mural SMC layers and increased leakiness.[19]

LLC transplants were established in syngeneic wild-type and *Cnn1*$^{-/-}$ mice. Compared with wild-type mice, the primary tumor growth was reduced in *Cnn1*$^{-/-}$ mice (Fig. 2a). Counting the CD31- or CD34-immunoreactive microvessels in vascular hot spots of LLC (microvessel density; MVD) revealed that there was a significant decrease in the MVD of tumors in *Cnn1*$^{-/-}$ mice compared with those in wild-type mice at 28 days of tumor transplantation (Fig. 2b). The decrease in MVD in *Cnn1*$^{-/-}$ mice was also observed in the size-matched tumors (approximately 600 mm^3) (Fig. 2b). To quantitatively assess the maturation status of the tumor vasculature, the number of microvessels covered by α-SMA-immunoreactive mural cells (pericytes or SMC) was determined for LLC at 12 and 28 days after transplantation. There was a striking difference in the percentage of capillaries associated with α-SMA-positive mural cells (MCI; mural cell-coverage index) between wild-type and *Cnn1*$^{-/-}$ tumor blood vessels at 28 days, with no difference at 12 days when the vasculatures were immature (Fig. 2c). In contrast to the wild-type mice, most capillaries in *Cnn1*$^{-/-}$ mice were enlarged (Fig. 2c), distorted and partially enveloped in less than 50% of the vessel surface by cells with α-SMA immunoreactivities. Blood vessels within B16 melanoma tumors generated in *Cnn1*$^{-/-}$ mice also showed reduced mural cell coverage and increased vascular diameter compared with those in wild-type mice (Fig. 2d). Immunohistochemical analysis using antibodies against CD34, α-SMA and a pericyte marker NG2 showed reduced mural cell coverage in the representative blood vessels in both the LLC and B16 melanoma xenografts in *Cnn1*$^{-/-}$ mice (Fig. 2e). Collectively, abnormalities in the morphology of tumor vasculature as well as the phenotype of normal vessels in brain and lung tissues by *Cnn1* deletion were characterized by reduced mural cell association with endothelium, indicating impaired maturation of blood vessels.[20]

Analysis of anti-α-SMA-immunostained (Fig. 3a) and anti-CD34-immunostained (data not shown) vessels in LLC tumors revealed that reduction of the MCI in the vasculature of *Cnn1*$^{-/-}$ mice was observed predominantly in the central region of tumors but not at the periphery or in the extra-tumor connective

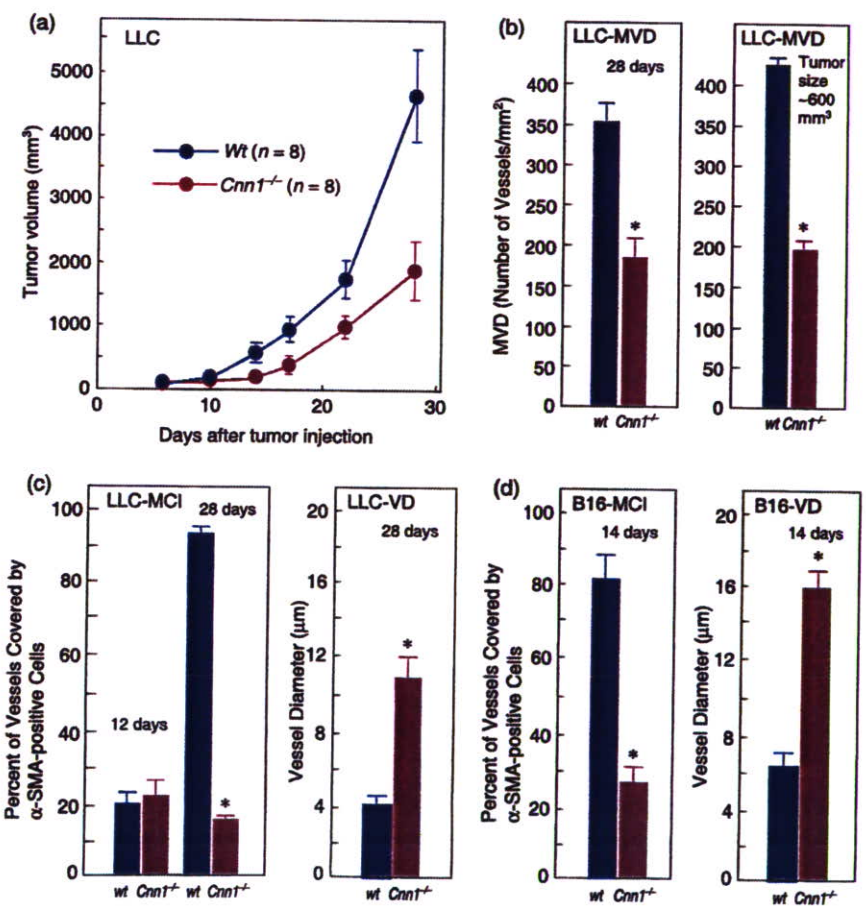

Fig. 2. Impaired maturation of blood vessels in tumor tissues in smooth muscle calponin-deficient (*Cnn1*)$^{-/-}$ mice. (a) Primary tumor growth of Lewis lung carcinoma (LLC) xenografts implanted into the flank (5×10^5 cells/mouse) was significantly reduced in *Cnn1*$^{-/-}$ mice. (b–d) Immunohistochemical analysis (CD31 or CD34, smooth muscle α-actin [α-SMA] and NG2) showed reduced microvessel densities (MVD) (b) and fraction of vessels with mural cell-coverage (MCI) of tumor blood vessels of LLC ($n = 4$) at 28 days after implantation and B16 melanoma (5×10^5 cells/mouse) ($n = 4$) at 14 days after implantation (c,d). The decrease in MVD in *Cnn1*$^{-/-}$ mice was also observed in the size-matched LLC tumors (approximately 600 mm^3). Blood vessels in both tumors also showed enlarged diameter (c,d). (e) Representative tumor vessels in wild-type and *Cnn1*$^{-/-}$ mice showed reduced MVD and MCI. Arrows indicate endothelial cells (black) and smooth muscle cells (SMC) (red). Scale bars = 50 μm. The data are mean ± SE (30 high-power field analyses per group). $^*P < 0.05$.

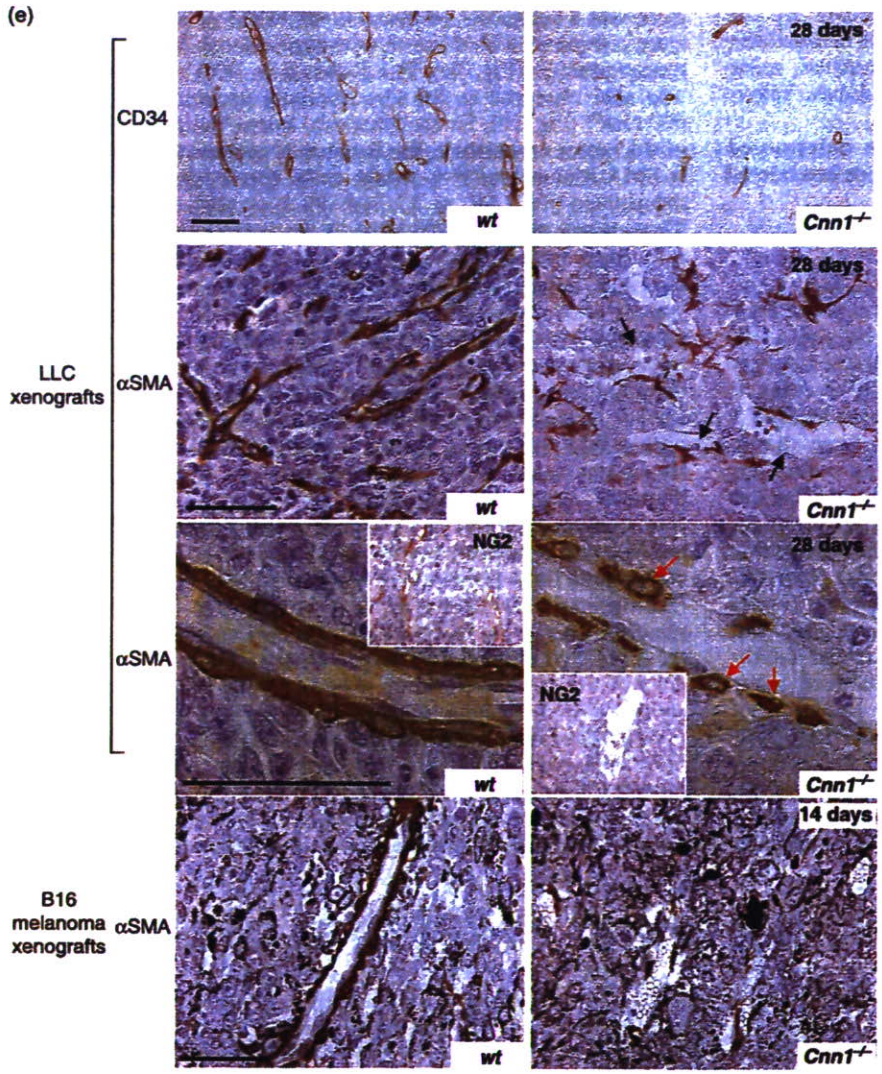

Fig. 2. *Continuet*

tissue (Fig. 3a,b). During the tumor-induced angiogenesis, *Cnn1* was normally expressed by peri-endothelial cells, most probably pericytes or SMC (Fig. 3c), as those *Cnn1*-positive cells were also positive for α-SMA (data not shown). Some of the *Cnn1*-positive cells in newly formed vasculature in both mouse (not shown) and human tumors (Fig. 3c) were proliferating. Previous studies suggest that for recruitment of the mural cells to angiogenic vasculature, their migration to the endothelium via PDGF-B and PDGFR-β signaling is functionally important.[17,18,20] *Cnn1* is involved in the force generation of actin and myosin in SMC.[2–4] We therefore investigated the effects of *Cnn1* deletion on PDGF-B-induced migration of vascular SMC *in vitro*, using the Boyden chamber analysis. As illustrated in Fig. 3d, both wild-type and *Cnn1*$^{-/-}$ SMC cultured from aorta were found to express PDGFR-β polypeptides, whereas only wild-type SMC expressed *Cnn1*. We also prepared *Cnn1*$^{-/-}$ SMC lines reconstituted with full-length *Cnn1* by adenovirus-mediated gene transfer (Fig. 3d). Analysis of migration revealed that approximately 45% less *Cnn1*$^{-/-}$ SMC than wild-type SMC migrated through a porous membrane coated with type I collagen in response to a gradient of PDGF-B, and also in its absence (Fig. 3e). Reconstitution of *Cnn1* expression by adenovirus reversed the inhibition of PDGF-B-induced migration of *Cnn1*$^{-/-}$ SMC up to levels that corresponded to wild-type SMC, whereas the inhibition of basal migration was not reversed. Thus, *Cnn1* deletion results in reduced chemotactic migration of SMC to PDGF-B.

Given the reduced mural cell association, implicating immaturity of blood vessels, it is likely that *Cnn1*$^{-/-}$ tumor vessels display VEGF-dependent remodeling of capillary structures, and endothelial and cancer cell survival.[21,22] We therefore tested whether the tumor vasculature in *Cnn1*$^{-/-}$ mice is sensitized to anti-angiogenesis treatment targeting VEGF. Implanted LLC cells in wild-type and *Cnn1*$^{-/-}$ mice were allowed to grow for 10 days, forming flank tumors ($n = 8$ each). Animals in the wild-type and *Cnn1*$^{-/-}$ groups were divided randomly and injections of mouse VEGF-specific neutralizing antibody or normal goat IgG were then given intraperitoneally twice a week for 2 weeks. Strikingly, at 18 days after initial anti-VEGF antibody injection, the treated tumors in *Cnn1*$^{-/-}$ mice were found to have prominent degeneration when compared with those in wild-type mice. Representative examples from macroscopic examination of the H&E-stained sections of the treated and untreated tumors are shown in Fig. 4a. It depicts extensive necrosis, vulnerability of immature vessels with hemorrhage, and more prominent obliteration of tumor vasculature in *Cnn1*$^{-/-}$ mice than in wild-type mice (Fig. 4b). An *in situ* apoptosis analysis (TUNEL) revealed that TUNEL-positive endothelial cells and cancer cells were rarely detected in untreated tumors in wild-type mice. In contrast, cancer cells transplanted in *Cnn1*$^{-/-}$ mice, even in untreated tumors, displayed significant propensity of apoptosis (Fig. 4c). In addition, the anti-VEGF antibody treatment increased TUNEL-positive endothelial cells more potently in *Cnn1*$^{-/-}$ mice

doi: 10.1111/j.1349-7006.2007.00452.x

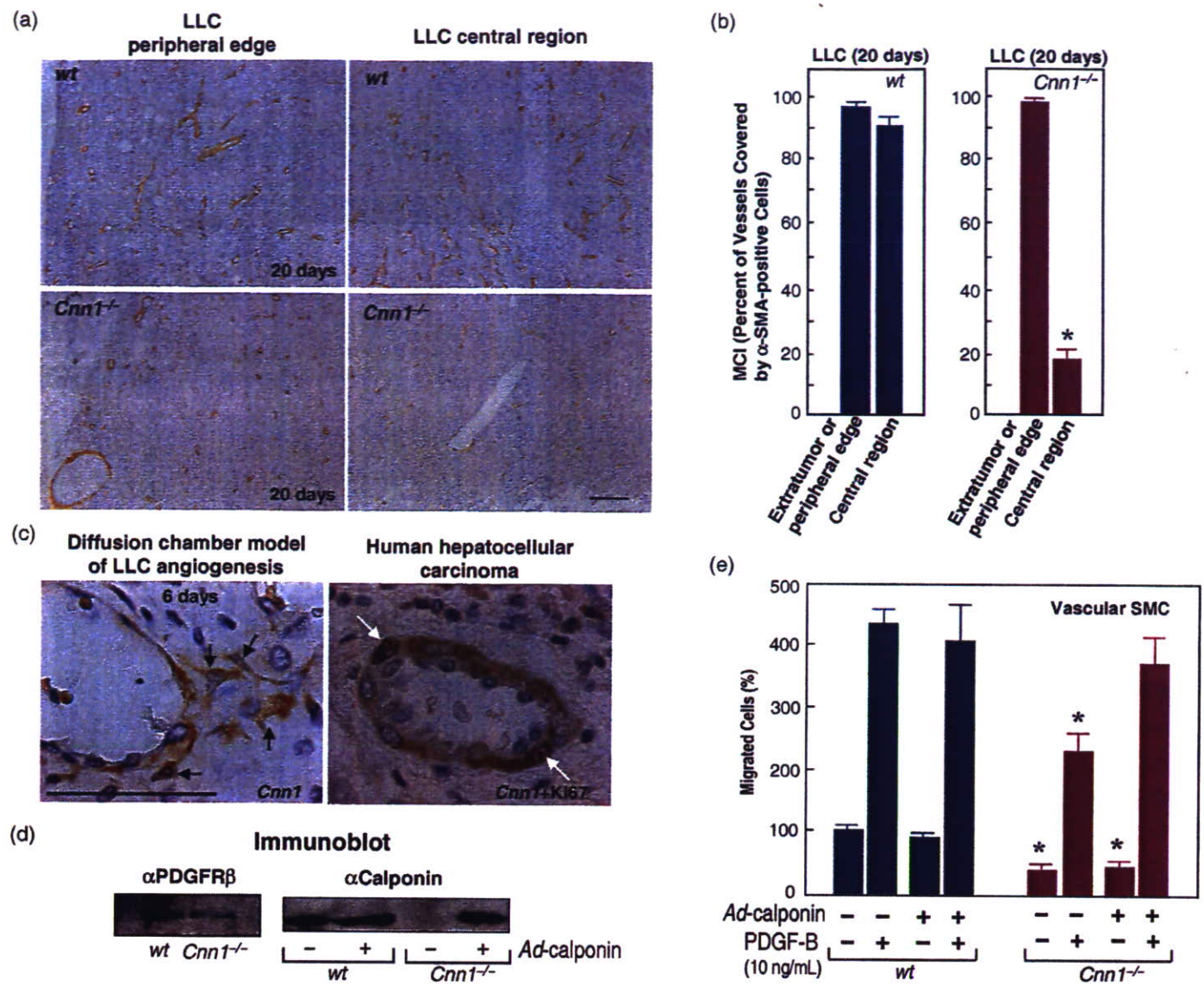

Fig. 3. (a,b) Prominent reduction of the mural cell-coverage (MCI) in smooth muscle calponin-deficient (*Cnn1*)$^{-/-}$ mice in the central region of tumors but not at the periphery of tumor tissues. Lewis lung carcinoma (LLC) xenografts were analyzed at 20 days after implantation (5×10^5 cells/mouse). Scale bar = 100 μm. (c) *Cnn1* was expressed in mural cells (black arrows) surrounding endothelial cells. Note the double staining of mural cells with *Cnn1* (cytoplasm) and Ki-67 (nucleus), an indicator of proliferating cells (white arrows). Scale bar = 50 μm. (d) Platelet-derived growth factor (PDGF) receptor β was expressed in both wild-type and *Cnn1*$^{-/-}$ mice, whereas *Cnn1* was expressed only in wild-type mice. Add-back of *Cnn1* expression in *Cnn1*$^{-/-}$ smooth muscle cells (SMC) was carried out by adenovirus-mediated transfection (multiplicity of infection = 30) of *Cnn1* cDNA. (e) Reduced SMC migration by *Cnn1* deletion. Inhibition of PDGF-B/B (10 ng/mL)-induced migration was compensated by the reconstitution of *Cnn1*, whereas random migration was not. The experiment was repeated twice, and the data are mean ± SE ($n = 4$ per group). *$P < 0.05$.

than in wild-type mice (data not shown). The anti-VEGF antibody can decrease MVD in both wild-type and *Cnn1*$^{-/-}$ mice (Fig. 4d). The MCI of the tumor vessels in *Cnn1*$^{-/-}$ mice increased significantly after treatment (Fig. 4e), indicating selective destruction of the fraction of vessels negative for α-SMA and normalization of tumor vasculature[23] (Fig. 4f). The results suggest that, under the experimental conditions used, reduced MCI in LLC tumor vasculature in *Cnn1*$^{-/-}$ mice may be caused by VEGF. The relationship between *Cnn1* deficiency and VEGF production in mural cells should be clarified in the future study. Moreover, consistent with the notion that angiogenesis inhibitors control tumor growth by increasing apoptosis of tumor cells, the anti-VEGF antibody was found to be more efficacious in killing pre-existing cancer cells in *Cnn1*$^{-/-}$ mice than in wild-type mice.

Assembly of mural cells to endothelial cells is well known to play a critical role in vessel maturation,[17,18,20–22] and it has been demonstrated that treatments targeted at killing both endothelial and mural cells are more effective in cancer treatment in preclinical animals.[22] Thus, an understanding of the molecular mechanism of mural cell recruitment to tumor endothelial cells is important for cancer treatment. However, genes as well as molecular pathways in mural cells controlling their assembly to the tumor vasculature are not fully understood. The results presented here, for the first time, demonstrate an important role for the *Cnn1* gene in vascular maturation at the tumor–host interface. Recent studies have demonstrated that knockdown of calponin in zebrafish blocks the proper migration of endothelial cells during formation of intersegmental vessels.[12] We now report that loss of *Cnn1* expression in SMC results in reduced chemotactic migration of SMC to PDGF-B, suggesting that it may cause defective SMC coverage of the tumor microvessels in *Cnn1*$^{-/-}$ mice. Our results also demonstrated that the properties of tissue

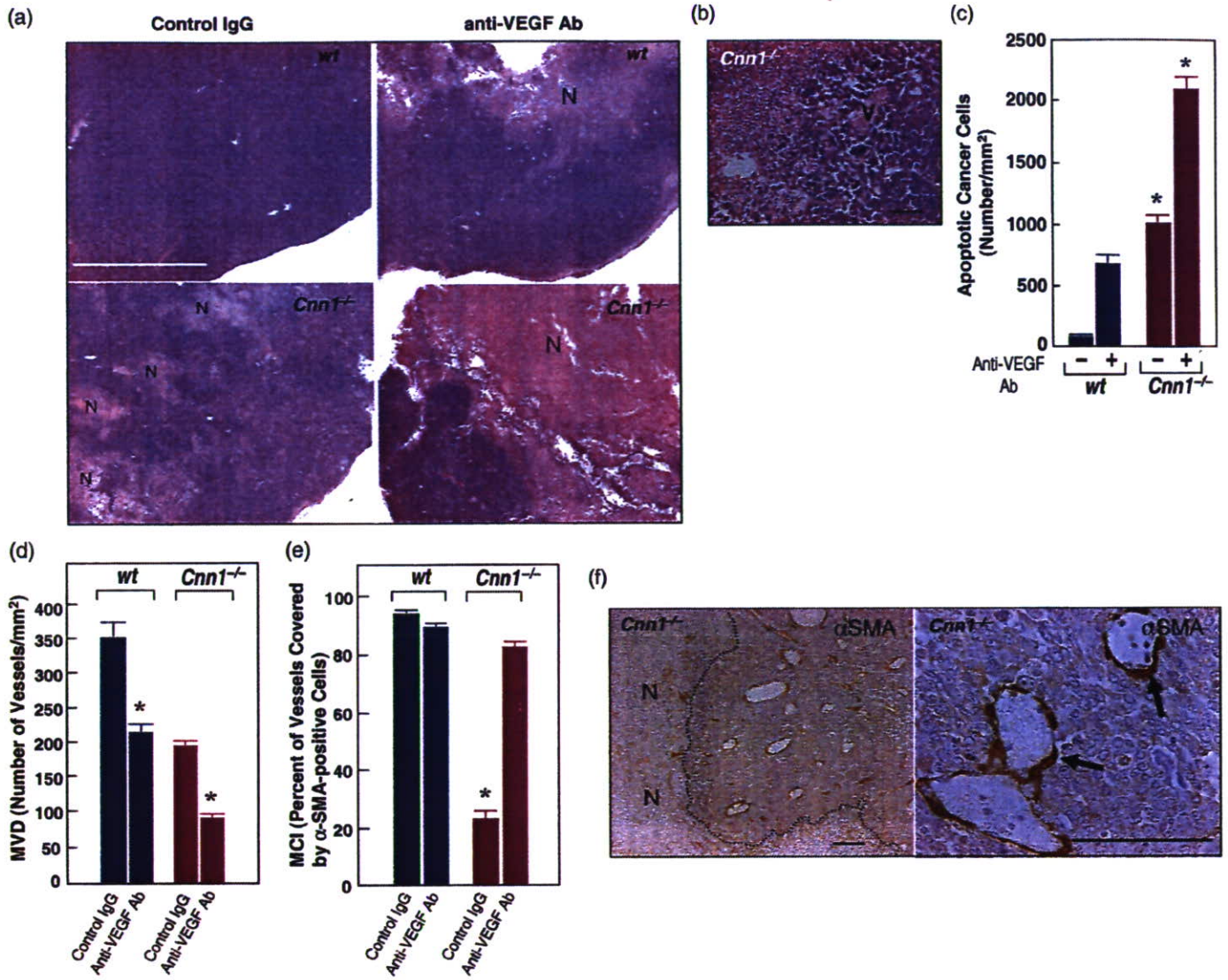

Fig. 4. Deletion of smooth muscle calponin (*Cnn1*)$^{-/-}$ leads to sensitization of cancer cells to anti-vascular endothelial growth factor (VEGF) antibody treatment. (a) Macroscopic view of hematoxylin–eosin (H&E)-stained sections of Lewis lung carcinoma (LLC) tumors 18 days after initial anti-angiogenesis therapy showed the most extensive necrosis of cancer cells (N) in anti-VEGF antibody-treated *Cnn1*$^{-/-}$ mice. Note that in *Cnn1*$^{-/-}$ mice, even non-treated tumor showed focal necrosis of cancer cells (N). White bar = 5 mm. (b) Higher magnification pictures show prominent destruction of tumor vasculature (V) in anti-VEGF antibody-treated LLC tumors in *Cnn1*$^{-/-}$ mice. Black bar = 50 μm. (c) Quantitation of TUNEL assay of tissue sections from the tumors in part (a), showing a striking increase in the number of apoptotic cancer cells in anti-VEGF antibody-treated LLC tumors in *Cnn1*$^{-/-}$ mice. Mean ± SE (30 high-power field analyses from four mice). *$P < 0.05$. (d–f) Treatment with anti-VEGF antibody significantly reduced the microvessel densities (MVD) in both wild-type and *Cnn1*$^{-/-}$ mice (d) and normalized the pericyte coverage index (PCI) in *Cnn1*$^{-/-}$ mice (e). Blood vessels covered by smooth muscle α-actin (α-SMA)-positive mural cells in *Cnn1*$^{-/-}$ mice were refractory to the anti-VEGF antibody therapy (f). Scale bar = 100 μm.

vasculature affected by *Cnn1* expression in mural cells play an important role in determining tumor phenotypes such as apoptosis and susceptibility to the treatment modalities.

Based on a current model of vessel assembly and remodeling,[20,21] our results imply that when tumor cells continue to express high levels of VEGF, reduced expression of *Cnn1* in local mural cells may lead to a rapid growth of leaky tumor vessels. Previous studies have demonstrated that when fluorescein is injected intravenously into mice, *Cnn1*$^{-/-}$ mice exhibit a greater and more rapid leakage of fluorecein from the blood vessels of the ocular fundus compared with wild-type mice.[19] These blood vessel phenotypes in *Cnn1*$^{-/-}$ mice may help to promote metastasis of the tumor cells as implicated by identification of *Cnn1* downregulation as a metastasis signature of solid tumors.[11] The *Cnn1*$^{-/-}$ phenotype of the host tissues, in fact, promotes lung metastasis of solid tumors.[19] We suggest that the status of vessel maturation evaluated by *Cnn1* expression in the mural cells of a given tumor may predict the efficacy of anti-angiogenesis treatments aimed at VEGF ablation, currently being used in the clinical stage.[21,22]

The finding that the vessel maturity changes in *Cnn1*$^{-/-}$ mice affect the vasculature in the central region of the tumor more than at the periphery and in the extra-tumor connective tissue raises the intriguing possibility that the effects may instead be due to a response to hypoxia of *Cnn1*$^{-/-}$ SMC at the tumor–host interface.

The results of the present study indicate that there is the potential for development of a new stromal therapy as a strategy for anticancer treatment. For example, viral replication controlled by the *Cnn1* promoter can destroy activated mural cells with *Cnn1* expression while sparing normal quiescent SMC.[24] We envision that, at least for certain human cancers with strong angiogenic capacity, combinatorial use of the viral agent target-

doi: 10.1111/j.1349-7006.2007.00452.x

ing mural cells may potentiate the efficacy of anti-VEGF antibody treatment. Prevention of vessel maturation in expanding tumors by silencing *Cnn1* expression may also be exploited for enforcing vessel regression via VEGF-withdrawal therapy, and may provide clues for solving the prevention of rarefaction of mature vessels that are refractory to VEGF in retinopathy of prematurity.[25]

Acknowledgments

This work was supported in part by Grants-in-Aids for Scientific Research from the Ministry of Education, Science, Sports and Culture, Japan, the Ministry of Health and Welfare, Japan, the Princes Takamatsu Cancer Research Fund (Tokyo).

References

1 Takahashi K, Hiwada K, Kokubu T. Vascular smooth muscle calponin: a novel troponin T-like protein. *Hypertension* 1988; **11**: 620–6.
2 Takahashi K, Yamamura H. Studies and perspectives of calponin in smooth muscle regulation and cancer gene therapy. *Adv Biophys* 2003; **37**: 91–111.
3 Matthew JD, Khromov AS, McDuffie MJ *et al.* Contractile properties and proteins of a calponin knockout mouse. *J Physiol (London)* 2000; **529**: 811–24.
4 Babu GJ, Celia G, Rhee AY *et al.* Effects of h1-calponin ablation on the contractile properties of bladder vs vascular smooth muscle in SM-B null mice. *J Physiol (London)* 2006; **577**: 1033–42.
5 Takahashi K, Nadal-Ginard B. Molecular cloning and sequence analysis of smooth muscle calponin. *J Biol Chem* 1991; **266**: 13 284–8.
6 Miano JM, Olsen EN. Expression of the smooth muscle cell calponin gene marks the early cardiac and smooth muscle cell lineages during mouse embryogenesis. *J Biol Chem* 1996; **271**: 7095–103.
7 Yamashita J, Itoh H, Hirashima M *et al.* Flk1-positive cells derived from embryonic stem cells serve as vascular progenitors. *Nature* 2000; **408**: 92–6.
8 Sasaki Y, Yamamura H, Kawakami Y *et al.* Expression of smooth muscle calponin in tumor vessels of human hepatocellular carcinoma and its possible association with prognosis. *Cancer* 2002; **94**: 1777–86.
9 Koganeshita Y, Takeoka M, Ehara T *et al.* Reduced expression of actin-binding proteins, h-caldesmon and calponin h1, in the vascular smooth muscle inside melanoma lesions: an adverse prognostic factor for malignant melanoma. *Br J Dermatol* 2003; **148**: 971–80.
10 Islam AH, Ehara T, Kato H *et al.* Calponin h1 expression in renal tumor vessels: correlation with multiple pathological factors of renal cell carcinoma. *J Urol* 2004; **171**: 1319–23.
11 Ramaswamy S, Ross KN, Lander ES, Golub TR. A molecular signature of metastasis in primary solid tumors. *Nature Genet* 2003; **33**: 49–54.
12 Tang J, Hu G, Hanai J *et al.* A critical role for calponin 2 in vascular development. *J Biol Chem* 2006; **281**: 6664–72.
13 Yoshikawa H, Taniguchi S, Yamamura H *et al.* Mice lacking smooth muscle calponin display increased bone formation that is associated with enhancement of bone morphogenetic protein responses. *Genes Cells* 1998; **3**: 685–95.
14 Eberhard A, Kahlert S, Goede V, Hemmerlein B, Plate KH, Augustin HG. Heterogeneity of angiogenesis and blood vessel maturation in human tumors: implication for antiangiogenic tumor therapies. *Cancer Res* 2000; **60**: 1388–93.
15 Morikawa S, Baluk P, Kaidoh T, Haskell A, Jain RK, McDonald DM. Abnormalities in pericytes on blood vessels and endothelial sprouts in tumors. *Am J Pathol* 2002; **160**: 985–1000.
16 Morioka T, Koyama H, Yamamura H *et al.* Role of h1-calponin in pancreatic AR42J cell differentiation into insulin-producing cells. *Diabetes* 2003; **52**: 760–6.
17 Lindahl P, Johansson BR, Leveen P, Betsholtz C. Pericyte loss and microaneurysm formation in PDGF-B-deficient mice. *Science* 1997; **277**: 242–5.
18 Hellstrom M, Kalen M, Lindahl P, Abramsson A, Betsholtz C. Role of PDGF-B and PDGFR-β in recruitment of vascular smooth muscle cells and pericytes during embryonic blood vessel formation in the mouse. *Development* 1999; **126**: 3047–55.
19 Taniguchi S, Takeoka M, Ehara T *et al.* Structural fragility of blood vessels and peritoneum in calponin h1-deficient mice, resulting in an increase in hematogenous metastasis and peritoneal dissemination of malignant tumor cells. *Cancer Res* 2001; **61**: 7627–34.
20 Jain RK, Booth MF. What brings pericytes to tumor vessels? *J Clin Invest* 2003; **112**: 1134–6.
21 Benjamin LE, Golijanin D, Itin A, Pode D, Keshet E. Selective ablation of immature blood vessels in established human tumors follows vascular endothelial growth factor withdrawal. *J Clin Invest* 1999; **103**: 159–65.
22 Bergers G, Song S, Meyer-Morse N, Bergsland E, Hanahan D. Benefits of targeting both pericytes and endothelial cells in the tumor vasculature with kinase inhibitors. *J Clin Invest* 2003; **111**: 1287–95.
23 Willet CG, Boucher Y, di Tomaso E *et al.* Direct evidence that the VEGF-specific antibody bevacizumab has antivascular effects in human rectal cancer. *Nature Med* 2004; **10**: 145–7.
24 Yamamura H, Hashio M, Noguchi M *et al.* Identification of the transcriptional regulatory sequences of human calponin promoter and their use in targeting a conditionally replicating herpes vector to malignant human soft tissue and bone tumors. *Cancer Res* 2001; **61**: 3969–77.
25 Keshet E. Preventing pathological regression of blood vessels. *J Clin Invest* 2003; **112**: 27–9.

JOURNAL OF VIROLOGY, Sept. 2007, p. 9653–9664
0022-538X/07/$08.00+0 doi:10.1128/JVI.00568-07

Vol. 81, No. 18

Enhanced Phosphorylation of Transcription Factor Sp1 in Response to Herpes Simplex Virus Type 1 Infection Is Dependent on the Ataxia Telangiectasia-Mutated Protein▽

Satoko Iwahori,[1] Noriko Shirata,[1] Yasushi Kawaguchi,[2] Sandra K. Weller,[3] Yoshitaka Sato,[1] Ayumi Kudoh,[1] Sanae Nakayama,[1] Hiroki Isomura,[1] and Tatsuya Tsurumi[1]*

Division of Virology, Aichi Cancer Center Research Institute, 1-1, Kanokoden, Chikusa-ku, Nagoya 464-8681, Japan[1]; Institute of Medical Science, University of Tokyo, Shirokanedai, Minato-ku, Tokyo 108-8639, Japan[2]; and Department of Molecular, Microbial and Structural Biology MC3205, University of Connecticut Health Center, 263 Farmington Avenue, Farmington, Connecticut 06030[3]

Received 19 March 2007/Accepted 26 June 2007

The ataxia telangiectasia-mutated (ATM) protein, a member of the related phosphatidylinositol 3-like kinase family encoded by a gene responsible for the human genetic disorder ataxia telangiectasia, regulates cellular responses to DNA damage and viral infection. It has been previously reported that herpes simplex virus type 1 (HSV-1) infection induces activation of protein kinase activity of ATM and hyperphosphorylation of transcription factor, Sp1. We show that ATM is intimately involved in Sp1 hyperphosphorylation during HSV-1 infection rather than individual HSV-1-encoded protein kinases. In ATM-deficient cells or cells silenced for ATM expression by short hairpin RNA targeting, hyperphosphorylation of Sp1 was prevented even as HSV-1 infection progressed. Mutational analysis of putative ATM phosphorylation sites on Sp1 and immunoblot analysis with phosphopeptide-specific Sp1 antibodies clarified that at least Ser-56 and Ser-101 residues on Sp1 became phosphorylated upon HSV-1 infection. Serine-to-alanine mutations at both sites on Sp1 considerably abolished hyperphosphorylation of Sp1 upon infection. Although ATM phosphorylated Ser-101 but not Ser-56 on Sp1 in vitro, phosphorylation of Sp1 at both sites was not detected at all upon infection in ATM-deficient cells, suggesting that cellular kinase(s) activated by ATM could be involved in phosphorylation at Ser-56. Upon viral infection, Sp1-dependent transcription in ATM expression-silenced cells was almost the same as that in ATM-intact cells, suggesting that ATM-dependent phosphorylation of Sp1 might hardly affect its transcriptional activity during the HSV-1 infection. ATM-dependent Sp1 phosphorylation appears to be a global response to various DNA damage stress including viral DNA replication.

Transcription factor Sp1 is a 95- to 105-kDa protein that binds to GC-rich recognition elements (GC-boxes) through C-terminal zinc finger motifs (30). Sp1 functions as a transactivator of gene expression, and its recognition elements are distributed widely in various promoters of cellular and viral genes (15, 16, 19). As with many other transcription factors, the transcription activity of Sp1 is regulated in part by post-translational modifications, which include phosphorylation, glycosylation, acetylation, and sumoylation (5, 9, 26, 54). It has been recently demonstrated that phosphorylation of Sp1 alters its transcription activity in a wide variety of physiological processes, including cell cycle progression, terminal differentiation, and viral infection (2, 9, 17, 23, 28, 36, 41). Also, relationships between the phosphorylation site(s) on Sp1 and specific kinases have been clarified, with documentation of targeting of Ser-59 by cyclin A-CDK, Ser-220 (quoted as Ser-131 in the original study) by DNA-dependent protein kinase (DNA-PK), Thr-453 and Thr-739 by p42/p44 mitogen-activated protein kinase (MAPK), and Thr-668 (quoted as Thr-579 in the original study) by casein kinase II (2, 9, 11, 17, 41). Cyclin A-CDK-mediated phosphorylation increases DNA-binding activity of Sp1 (17, 23). Inactivation of Thr-453 and Thr-739 phosphorylation sites by p42/p44 MAPK decreases by half the transcriptional activity (41). Mutation of the Thr-668 phosphorylation site which is in the Zinc finger motif of Sp1 increases its DNA-binding activity, further suggesting that casein kinase II-mediated phosphorylation decreases DNA-binding activity of Sp1 (2).

Phosphorylation of Sp1 upon virus infection has been reported in several studies (9, 11, 28, 31). For example, simian virus 40 infection induces both increased levels and phosphorylation of Sp1 (28). In a study of human immunodeficiency virus type 1 (HIV-1) infection, it was shown that the HIV-1-encoded Tat protein promotes DNA-PK-dependent Sp1 phosphorylation in vitro, which is associated with increased transcription activity (11).

Herpes simplex virus type 1 (HSV-1) is a large, enveloped virus with 152-kbp double-stranded DNA encoding approximately 84 proteins (39, 49). During productive replication, cascade regulation of gene expression occurs, based on stepwise activation of immediate-early, early, early late, and late promoters (24). The promoters of different expression kinetics classes are equipped for binding of not only viral transcription factors but also various cellular transcription factors, including Sp1. Sp1-binding sites are frequently found in promoters of immediate-early and early genes (48, 57), suggesting a pivotal

* Corresponding author. Mailing address: Division of Virology, Aichi Cancer Center Research Institute, 1-1, Kanokoden, Chikusa-ku, Nagoya 464-8681, Japan. Phone and fax: 81-52-764-2979. E-mail: ttsurumi@aichi-cc.jp.

▽ Published ahead of print on 3 July 2007.

function of Sp1 in gene expression of HSV-1. HSV-1 infection induces hyperphosphorylation of Sp1 at early stages of infection without any significant change in abundance (31). While the DNA-binding activity of Sp1 was found to be unchanged until 8 h postinfection (hpi), purified Sp1 from HSV-1-infected cells at 12 hpi had reduced transcription activity in vitro (31). However, the kinase(s) responsible for Sp1 phosphorylation induced by HSV-1 infection have remained unclear.

We and others previously reported that HSV-1 infection induces a cellular DNA damage response, with activation of the ATM signal transduction pathway (37, 53, 60). The activated form of ATM phosphorylated at Ser-1981 and the DNA damage sensor Mre11-Rad50-Nbs1 complex are recruited and retained in viral replication compartments, where transcription and replication of viral genes take place. Activation of the ATM-Rad3-related (ATR) replication checkpoint pathway, in contrast, is minimal. ATM is a member of the related phosphatidylinositol 3 (PI-3)-like kinase family, as well as ATR and DNA-PK, and displays kinase activity against serine and threonine, followed by glutamine, generally responding to a genotoxic stress such as ionizing radiation (IR) (1, 6, 12, 13, 52).

In the present report, we provide evidence for considerable ATM involvement in the hyperphosphorylation of Sp1 during HSV-1 infection rather than individual HSV-1-encoded PKs. In ATM-deficient cells or cells silenced for ATM expression by short hairpin RNA (shRNA) targeting, the levels of the hyperphosphorylated form of Sp1 did not increase even as HSV-1 infection progressed. Using mutational analysis and immunoblotting with phosphopeptide-specific antibodies, we have identified that at least Ser-56 and Ser-101 on Sp1 became phosphorylated in response to HSV-1 infection. Although ATM phosphorylated Ser-101 but not Ser-56 on Sp1 in vitro, phosphorylation of Sp1 at both sites was not detected at all upon infection in ATM-deficient cells, suggesting that other cellular kinase(s) activated by ATM could be involved in phosphorylation at Ser-56. Upon viral infection Sp1-dependent transcription in ATM expression-silenced cells was almost the same as that in ATM-intact cells, suggesting that ATM-dependent phosphorylation of Sp1 might hardly affect its transcriptional activity during viral infection. Since it is known that HSV-1 infection decreases transcriptional activity of Sp1 (31), modification(s) of Sp1 besides ATM-dependent phosphorylation might affect its transcriptional activity.

MATERIALS AND METHODS

Cells. HeLa, HFF2 (human foreskin fibroblasts immortalized by introduction of the human telomerase reverse-transcriptase [*hTERT*] gene [56]), and 293T cells were grown and maintained at 37°C in Dulbecco modified Eagle medium (DMEM; Sigma) supplemented with 10% fetal calf serum (FCS). Human glioma cell lines M059J and MJ-M6 (34) were maintained in DMEM–Ham F-12 nutrient mixture (Sigma) supplemented with 10% FCS and puromycin (0.5 μg/ml). Skin fibroblasts from ataxia telangiectasia patients immortalized by introduction of *hTERT* gene (AT10S/T-n cells) were maintained at 37°C in DMEM supplemented with 10% FCS and G418 (200 μg/ml) (43). The 293T cells were infected with retroviruses expressing ATM shRNA or control retroviruses and selected (56). The resultant 293T cells stably expressing ATM shRNA (293T-ATM shRNA) or the control vector cells (293T-Control vector) were maintained at 37°C in DMEM supplemented with 10% FCS and hygromycin B (100 μg/ml) (56). Sf9 and SF21 cells were maintained at 27°C in Sf-900 II (Gibco) supplemented with 10% FCS.

Viruses. HSV-1 strain 17+ was used throughout the experiments. A Us3-deficient virus, R7041 (46), and a UL13-deficient virus, R7356 (47), derived from HSV-1 strain F were kindly provided by B. Roizman. The UL39-deficient virus, ICP6Δ, derived from HSV-1 strain KOS was from a collaborator, S. K. Weller (20). Infection was performed on monolayers of cultured cells at the indicated multiplicities of infection (MOIs). After 1 h adsorption at 37°C, inoculum was removed, and monolayers were overlaid with fresh medium.

TABLE 1. Primer sets for construction of serine/threonine-to-alanine mutations by site-directed mutagenesis

Mutation site	Sequences of paired primers (5′–3′)
S36A	GGTGGTGCCTTTGCACAGGCTCGAA
	TTCGAGCCTGTGCAAAGGCACCACC
S56A	GGAGGGCAGGAGGCCCAGCCATCCC
	GGGATGGCTGGGCCTCCTGCCCTCC
S81A	AGAACAGCAACAACGCCCAGGGCCCGAGTC
	GACTCGGGCCCTGGGCGTTGTTGCTGTTCT
S85A	CTCCCAGGGCCCGGCTCAGTCAGGGGGAAC
	GTTCCCCCTGACTGAGCCGGGCCCTGGGAG
T98A	GACCTCACAGCCGCACAACTTTCAC
	GTGAAAGTTGTGCGGCTGTGAGGTC
S101A	GCCACACAACTTGCACAGGGTGCCA
	TGGCACCCTGTGCAAGTTGTGTGGC
T250A	CTCTCAGGACAGGCTCAGTATGTGA
	TCACATACTGAGCCTGTCCTGAGAG
S281A	CCTTGACTCCCAGCGCTCAGGCAGTCACGA
	TCGTGACTGCCTGAGCGCTGGGAGTCAAGG
S291A/S296A	AGCAGCTCTGGGGCCCAGGAGAGTGGCGC
	ACAGCCTGTCA
	TGACAGGCTGTGCGCCACTCTCCTGGGCCCC
	AGAGCTGCT
S313A	AGCTTGGTATCAGCACAAGCCAGTT
	AACTGGCTTGTGCTGATACCAAGCT
S351A	TCAGGGACCAACGCTCAAGGCCAGA
	TCTGGCCTTGAGCGTTGGTCCCTGA
T394A	CAAAACCAGCAGGCACAGCA
	TGCTGTGCCTGCTGGTTTTG
T427A/S431A	GGGCAGACCTTTGCAGCTCAAGCCATCGCC
	CAGGAAACCC
	GGGTTTCCTGGGCGATGGCTTGAGCTGCAA
	AGGTCTGCCC

Plasmids. For subcloning of Sp1 gene into pFastBac1 (Invitrogen) containing a sequence (RGS-6xHis-Flag) supplied by W. Nakai, two primers (5′-GGAAT TCCATATGGATGAAATGACAGCTGTGG-3′ and 5′-GCTCTAGATCAGA AGCCATTGC-3′) were designed. Plasmid CMV-hSp1 (22) supplied from G. Suske was used as a template for PCR. The PCR product was double digested by NdeI and XbaI and subcloned into pFastBac1 containing a sequence (RGS-6xHis-Flag), and the resultant plasmid was designated pFB-RHF/Sp1. For construction of a mammalian expression vector for Sp1, two primers (5′-TTATAA TAGGGGTACCCCACCATGCGCGG-3′ and 5′-GCTCTAGAGCTCAGAAG CCA-3′) were designed. pFB-RHF/Sp1 was used as a template for PCR. The PCR product was double digested by KpnI and XbaI and subcloned into pcDNA3.1(+) (Invitrogen), and the resultant plasmid was designated pcDNA-RHF/Sp1. Serine/threonine-to-alanine mutations were constructed with a QuikChange site-directed mutagenesis kit (Stratagene) using the primer sets given in Table 1. Multiple mutations were introduced by repetition. The plasmids were designated pcDNA-RHF/Sp1-S36A, pcDNA-RHF/Sp1-S56A, pcDNA-RHF/Sp1-S81A, pcDNA-RHF/Sp1-S85A, pcDNA-RHF/Sp1-T98A, pcDNA-RHF/Sp1-S101A, pcDNA-RHF/Sp1-T250A/S281A, pcDNA-RHF/Sp1-S291/296A, pcDNA-RHF/Sp1-S313A, pcDNA-RHF/Sp1-S351A, pcDNA-RHF/Sp1-T394A, pcDNA-RHF/Sp1-T427A/S431A, pcDNA-RHF/Sp1-S56/81/85A, pcDNA-RHF/Sp1-S56/101A, pcDNA-RHF/Sp1-S56A/T250A, and pcDNA-RHF/Sp1-S56/281A, and all mutations were confirmed by sequencing.

For subcloning of a glutathione *S*-transferase (GST) fusion protein with truncated Sp1 (8 to 167 amino acids), two primers (5′-CGGGATCCCGTATGGAT GAAATGAC-3′ and 5′-ACTCTCGAGCACTCCAGGTAGT-3′) were designed, and pcDNA-RHF/Sp1, pcDNA-RHF/Sp1-S56A, pcDNA-RHF/Sp1-S101A, and pcDNA-RHF/Sp1-S56/101A were used as templates for PCR. The PCR products were double digested with BamHI and XhoI and subcloned into pGEX-6P-3 (Amersham Biosciences). The plasmids were designated pGEX-6P-$Sp1_{8\text{-}167}$, pGEX-6P-$Sp1_{8\text{-}167}$-S56A, pGEX-6P-$Sp1_{8\text{-}167}$-S101A, and pGEX-6P-$Sp1_{8\text{-}167}$-S56/101A.

Purification of recombinant Sp1 from insect cells. Purification of recombinant His_6 flag-tagged Sp1 from insect cells was carried out with a Bac-to-Bac system (Invitrogen). DH10Bac *Escherichia coli* cells were transformed with pFB-RHF/

Sp1, and the resultant bacmid was transfected into Sf9 cells using Lipofectin reagent (Invitrogen). The obtained virus was designated AcRHF/Sp1. SF21 cells (5×10^7) were infected with AcRHF/Sp1 at an MOI of 5. At 60 hpi, the cells were harvested, suspended in a buffer (50 mM Tris-HCl [pH 8], 1% Nonidet P-40 [NP-40], 250 mM NaCl, 10 mM 2-mercaptoethanol [2-ME], 1 mM phenylmethylsulfonyl fluoride [PMSF]), sonicated, and centrifuged. The clarified lysate was combined with Ni-NTA (QIAGEN). After rotation for 2 h, the beads were washed twice with buffer A (20 mM Tris-HCl [pH 8], 10% glycerol, 10 mM 2-ME) containing 500 mM KCl and 20 mM imidazole, once with buffer A containing 1 M KCl, once with buffer A containing 500 mM KCl and 20 mM imidazole, and twice with buffer A containing 100 mM KCl and 20 mM imidazole and then eluted with buffer A containing 100 mM KCl and 100 mM imidazole. The eluted protein was dialyzed against dialysis buffer (20 mM Tris-HCl [pH 8], 100 mM NaCl, 20% glycerol, and 1 mM PMSF) and combined with anti-Flag M2 affinity gel (Sigma). After rotation for 3 h, the beads were washed three times with TBS+ buffer (50 mM Tris-HCl [pH 8], 150 mM NaCl, 1 mM EDTA, 0.1% NP-40, 10% glycerol, 1 mM PMSF), and the protein was eluted with 0.1 M glycine (pH 3.5), neutralized immediately, dialyzed against dialysis buffer, and stored at −80°C.

Purification of recombinant Sp1 from bacteria. *E. coli* (BL21) transformed with pGEX-6P-$Sp1_{8-167}$, pGEX-6P-$Sp1_{8-167}$-S56A, pGEX-6P-$Sp1_{8-167}$-S101A, and pGEX-6P-$Sp1_{8-167}$-S56/101A were cultured at 30°C until the optical density at 600 nm reached 0.6, and IPTG (isopropyl-β-D-thiogalactopyranoside) was added at a final concentration of 1 mM. After 5 h of incubation, the collected cells were suspended in GLB buffer (50 mM Tris-HCl [pH 7.4], 50 mM glucose, 1 mM EDTA, 10 mM 2-ME, 1 mM PMSF, 0.2% NP-40). After sonication, the lysate was clarified by centrifugation, combined with glutathione-Sepharose 4B (Amersham Biosciences), and rotated at 4°C for 90 min. After three washes with GLB containing 0.2% NP-40, the proteins were eluted with elution buffer (10 mM reduced glutathione, 50 mM Tris-HCl [pH 8], 1 mM PMSF) and dialyzed against dialysis buffer. The purified proteins were designated GST-$Sp1_{8-167}$, GST-$Sp1_{8-167}$-S56A, GST-$Sp1_{8-167}$-S101A, and GST-$Sp1_{8-167}$-S56/101A.

IP-kinase assays. Immunoprecipitation (IP)-kinase assays were performed with some modification as described previously (6, 10, 32). 293T cells (5×10^6) were transfected with either pcDNA-Flag-ATMwt or pcDNA-Flag-ATMkd (5 μg of each; kind gifts from M. B. Kastan [6]) using Lipofectamine 2000 (Invitrogen). At 48 h posttransfection, cells were harvested, rinsed with ice-cold phosphate-buffered saline, lysed with lysis buffer (20 mM Tris-HCl [pH 7.4], 150 mM NaCl, 1 mM EDTA, 0.5% Triton X-100 [TX-100], 5% glycerol, 1 mM PMSF, 100 mM NaF, 2 mM Na_3VO_4, and complete protease inhibitor [Roche]), incubated for 15 min on ice, sonicated, and clarified by centrifugation. Cell lysates (2 mg) were incubated with anti-Flag M2 affinity resin (20 μl of suspension) and rotated for 3 h at 4°C. The immunocomplex was washed three times with lysis buffer containing 0.65% TX-100, twice with Tris-LiCl buffer (100 mM Tris-HCl [pH 7.5], 0.5 M LiCl, 1 mM NaF, 1 mM Na_3VO_4) and once with kinase buffer (10 mM HEPES [pH 7.9], 50 mM glycerophosphate, 50 mM NaCl, 10 mM $MgCl_2$, 10 mM $MnCl_2$, 1 mM dithiothreitol, 1 mM NaF, and 1 mM Na_3VO_4) containing 5 μM ATP. For activation of ATM, the immunocomplex was incubated with kinase buffer containing 1 mM ATP for 30 min at 30°C. After incubation, the immunocomplex was washed three times with kinase buffer containing 5 μM ATP and divided into two portions for kinase reactions with either purified Sp1 or p53 as substrate. Kinase reactions were carried out by resuspending the immunocomplex in kinase buffer containing 10 μCi [γ-^{32}P]ATP and either 500 ng of Sp1 purified from insect cells or 250 ng of p53 (Active Motif), followed by incubation for 30 min at 30°C. The reactions were terminated by addition of sodium dodecyl sulfate (SDS) gel loading buffer, and the samples were separated by SDS–10% polyacrylamide gel electrophoresis (PAGE), followed by autoradiography. In the case of GST-$Sp1_{8-167}$, GST-$Sp1_{8-167}$-S56A, GST-$Sp1_{8-167}$-S101A, and GST-$Sp1_{8-167}$-S56/101A, 1 μg of each protein was used as a substrate.

Antibodies. Primary antibodies were purchased from Santa Cruz (Sp1 PEP2), Abcam (HSV-1 ICP4, UL42), GeneTex (ATM-2C1), Cell Signaling Technology (ATM-S1981), Ambion (GAPDH [glyceraldehyde-3-phosphate dehydrogenase]), Sigma (Flag M2), and Biosource (DNA-dependent PK catalytic subunit). Phosphopeptide-specific rabbit antibodies were raised against serine-56 phosphopeptide, CGGGQEpSQPSPL, for anti-Sp1 (pS56) and serine-101 phosphopeptide, CTATQLpSQGANG, for anti-Sp1 (pS101), conjugated with KLH. Antibodies were purified through the specific phosphopeptide-conjugated columns and passed through the corresponding unphosphorylated peptide-conjugated columns.

Transient-transfection and infection. HeLa cells (6×10^5) were transfected with 0.8 μg of pcDNA-RHF/Sp1 or expression vectors of mutated Sp1 using Lipofectamine 2000. At 24 h posttransfection, the transfected cells were infected with HSV-1 at an MOI of 10. At 24 hpi, the cells were harvested and subjected to immunoblot analysis.

IP. HeLa cells transfected with pcDNA-RHF/Sp1, pcDNA-RHF/Sp1-S56A, or pcDNA-RHF/Sp1-S101A were infected with HSV-1 at an MOI of 10. At 24 hpi, the cells were harvested, suspended in lysis buffer (50 mM Tris-HCl [pH 7.4], 150 mM NaCl, 1 mM EDTA, 1% TX-100, 100 mM NaF, 2 mM Na_3VO_4, and protease inhibitor cocktail [Sigma]), and centrifuged. The clarified lysate was combined with anti-Flag M2 affinity resin and rotated for 3 h at 4°C. The immune complex was washed three times with TBS buffer (50 mM Tris-HCl [pH 7.4], 150 mM NaCl), and eluted with SDS gel loading buffer.

Immunoblot analysis. HeLa, HFF2, M059J, MJ-M6, and AT10S/T-n cells were suspended in lysis buffer (20 mM Tris-HCl [pH 7.4], 0.5% TX-100, 300 mM NaCl, 1 mM EDTA, 0.1% SDS, 100 mM NaF, 2 mM Na_3VO_4, protease inhibitor cocktail [Sigma]) and incubated on ice for 40 min, followed by centrifugation to obtain clarified supernatants. 293T-ATM shRNA and 293T-Control vector cells were suspended in urea buffer (8 M urea, 0.1 M NaH_2PO_4, 10 mM Tris [pH 8]), sonicated, and centrifuged. For experiments with alkaline phosphatase treatment, HFF2 and HeLa cells were infected with HSV-1 and harvested at 10 and 12 hpi, respectively. Cells were suspended in AP buffer (50 mM Tris-HCl [pH 8], 0.5 M NaCl, 2% NP-40, protease inhibitor cocktail [Sigma]), stored on ice for 30 min, and then centrifuged. Whole-cell lysates (20 μg) were incubated in a reaction mixture containing 10 U of calf intestinal alkaline phosphatase (CIAP; New England Biolabs) and 10 mM $MgCl_2$ for 30 min at 37°C. Equal amounts of proteins (2.5 to 30 μg) were separated by 7.5% (acrylamide [A]:bisacrylamide [B] = 72:1) or 10% (A:B = 30:0.8) SDS-PAGE and transferred onto Immobilon transfer membranes (Millipore). Immunoreactivity was detected by Western Lightning (Perkin-Elmer). Images were processed by LumiVision PRO 400EX (Aisin/Taitec, Inc.). Signal intensity was quantified with LumiVision Analyzer 400. The system used in the present study mounts the cooled charge-coupled device camera that has 16 bit = 65,535 grayscale wide dynamic range. It enhances the accuracy of the quantitative analysis up to 100 times compared to the ordinary quantitative analysis scanning an X-ray film into the personal computer after exposing the signal to the film.

IR. HFF2 cells were exposed to gamma irradiation with 10 Gy and harvested at 15 min after radiation. 293T-ATM shRNA and 293T-Control vector cells were exposed to gamma irradiation with 20 Gy and harvested at 15 min after radiation.

CAT assays. Chloramphenicol acetyltransferase (CAT) assays were carried out as described previously (27, 62). All transfections were in triplicate on 35-mm-diameter plates of 293T-ATM shRNA or 293T-Control vector cells (1.2×10^6) with either p65F1CAT (3.5 μg; a gift from A. D. Yurochko) (62) or pCAT TATA+Sp1(−55)+Sp1 (−75) (1 μg) (27) using Lipofectamine 2000 according to the manufacturer's instructions. At 24 h posttransfection, cells were infected with HSV-1 at an MOI of 5 and harvested at 12 hpi. Cell lysates were then prepared and subjected to CAT assays as described previously (27, 62). Equal amounts of proteins from each sample [0.4 μg for p65F1CAT-transfected cells, 0.2 μg for pCAT TATA+Sp1(−55)+Sp1(−75)-transfected cells] were assayed for CAT activity. Acetylated and unacetylated [^{14}C]chloramphenicol (Amersham Biosciences) were separated by thin-layer chromatography in a chloroform-methanol (95:5) solvent. Images were obtained using a BAS2500 Image Reader (Fujifilm), the signal intensities were quantified with an Image Gauge, and the levels of activity were analyzed by calculating the percentage of the conversion of unacetylated [^{14}C]chloramphenicol to the acetylated form.

RESULTS

Hyperphosphorylation of Sp1 is induced upon HSV-1 infection. In order to confirm whether transcription factor Sp1 is hyperphosphorylated upon HSV-1 infection as reported previously (31), HeLa and HFF2 cells were infected with HSV-1. As shown in Fig. 1A, most of the Sp1 proteins were converted to slower-migrating forms in SDS-PAGE by 4 hpi in HeLa cells. Similarly, the slower-migrating forms of Sp1 in HFF2 cells became the major form by 4 hpi (Fig. 1C). CIAP treatment of the lysates from HSV-1-infected HeLa cells (Fig. 1B) or HFF2 cells (Fig. 1D) changed the slower-migrating forms of Sp1 to the faster-migrating form. Thus, Sp1 became hyperphosphorylated after HSV-1 infection without a significant change in abundance, confirming the previous finding (31).

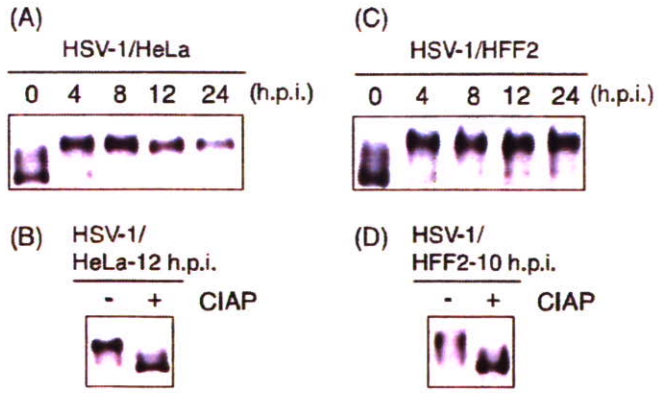

FIG. 1. Hyperphosphorylation of Sp1 is induced upon HSV-1 infection. HeLa (A) and HFF2 cells (C) were infected with HSV-1 at MOIs of 10 and 5, respectively, and were harvested at the indicated times postinfection. Whole-cell lysates were prepared, and equal amounts of proteins from each sample (2.5 or 30 μg) were subjected to immunoblot analysis with anti-Sp1 antibody. (B and D) Whole-cell lysates obtained from HSV-1-infected HeLa and HFF2 cells at the indicated times postinfection were treated with (+) or without (−) CIAP for 30 min at 37°C. The samples were subjected to immunoblot analysis with anti-Sp1 antibody.

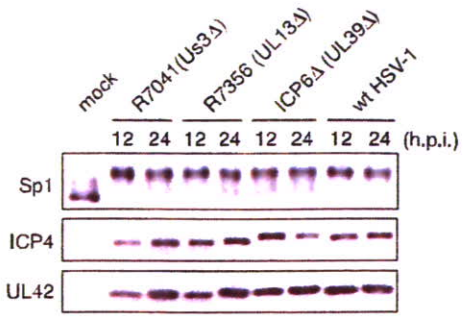

FIG. 2. Hyperphosphorylation of Sp1 is induced even upon infection of HSV-1 mutants defective for viral PK, Us3, UL13 or UL39 gene product. HFF2 cells were infected with wild-type HSV-1 (wt HSV-1), Us3-defective virus (R7041), UL13-defective virus (R7356), or UL39-defective virus (ICP6Δ) at an MOI of 5. At 12 and 24 hpi, cells were harvested and whole-cell lysates were prepared. Equal amounts of proteins from each sample (15 μg) were subjected to immunoblot analysis with anti-Sp1, ICP4, and UL42 proteins specific antibodies. Mock, mock infection.

Hyperphosphorylation of Sp1 is induced even upon infection of HSV-1 mutants defective for viral PK, Us3, UL13, or UL39 gene product. HSV-1 expresses at least three viral PKs encoded by the Us3, UL13, and UL39 genes (20, 46, 47). To examine whether Us3, UL13, or UL39 viral PK is involved in the Sp1 hyperphosphorylation, we investigated the phosphorylation state of Sp1 in HFF2 cells infected with wild type, Us3-deficient (R7041), UL13-deficient (R7356), or UL39 (viral ribonucleotide reductase large subunit)-deficient (ICP6Δ) virus (Fig. 2). The expression levels of the virus-encoded immediate-early protein (ICP4) and early protein (UL42) were almost the same among wild-type- and the mutant virus-infected cells. Since R7041 and R7356 are derived from HSV-1 strain F (46, 47) and ICP6Δ is from HSV-1 strain KOS (20), it is possible that the different gel mobilities of ICP4 proteins among wild-type HSV-1 (strain 17+) and the mutant viruses could be due to interstrain variabilities. Sp1 proteins in HFF2 cells infected with Us3-deficient (R7041), UL13-deficient (R7356), or UL39-deficient (ICP6Δ) viruses were mainly detected as hyperphosphorylated forms (the slower-migrating forms) by 12 hpi, as in the case of wild-type HSV-1 (Fig. 2). These results indicate that HSV-1 encoded PKs are not individually involved to any large extent in Sp1 hyperphosphorylation induced upon HSV-1 infection. However, the possibility of redundancy among some combination of these three PKs in Sp1 phosphorylation could not be excluded.

Activated ATM is involved in hyperphosphorylation of Sp1 upon HSV-1 infection. The HSV-1 infection activates ATM and elicits an ATM-dependent DNA damage signal transduction in infected cells (37, 53, 60). Since Sp1 possesses 15 putative phosphorylation sites targeted by ATM as estimated from the motifs (see Fig. 5A), we therefore examined phosphorylation states of Sp1 in ATM expression-silenced 293T cells infected with HSV-1 (Fig. 3A). The 293T cells stably expressing the ATM gene-targeted shRNA (293T-ATM shRNA) or the control vector cells (293T-Control vector) (53, 56) were infected with HSV-1. The expression level of ATM was very low in 293T-ATM shRNA cells compared to that in 293T-Control vector cells. In 293T-Control vector cells, most of the Sp1 proteins were hyperphosphorylated to slower-migrating forms by 5 hpi (Fig. 3A). In contrast, in 293T-ATM shRNA cells part of the Sp1 protein was converted to hyperphosphorylated forms, but 44% of Sp1 still remained as the faster-migrating form even at 24 hpi. It should be noted that the expression profiles of an immediate-early protein, ICP4, and an early protein, UL42, were almost the same between both cell lines, although the phosphorylation state of Sp1 was considerably different. Furthermore, as shown in Fig. 3B, in ATM-deficient AT10S/T-n cells from ataxia telangiectasia patients (43), Sp1 was originally present mostly as the faster-migrating form and only partially as the slower-migrating forms. The conversion efficiency from the faster-migrating form to slower-migrating forms was low in HSV-1-infected AT10S/T-n cells, as well as the case with ATM expression-silenced 293T cells. These observations strongly suggest that ATM is involved directly or indirectly in Sp1 hyperphosphorylation upon HSV-1 infection.

To further confirm the relationship between Sp1 hyperphosphorylation and ATM activation, the phosphorylation states of Sp1 were also compared in the human glioma cell lines M059J, which is DNA-dependent PK catalytic subunit (DNA-PKcs) null, and MJ-M6, which is a DNA-PKcs revertant of M059J cells transfected with the full-length DNA-PKcs cDNA expression vector (34) (Fig. 3C). It was previously shown that DNA-PKcs-deficient cells express very low levels of ATM and that recovery of DNA-PKcs partially restores ATM expression levels (25, 45). In MJ-M6 cells, the slower-migrating forms of Sp1 began to increase from 5 hpi, and almost all Sp1 proteins were converted to hyperphosphorylated forms by 10 hpi, appearing to correlate with expression levels of the activated ATM phosphorylated at Ser-1981. No change in the amount of ATM protein occurred throughout HSV-1 infection, whereas the levels of DNA-PKcs protein significantly decreased by 5 hpi. As previously reported, the degradation is dependent on the expression of the virus-encoded immediate-early protein ICP0,

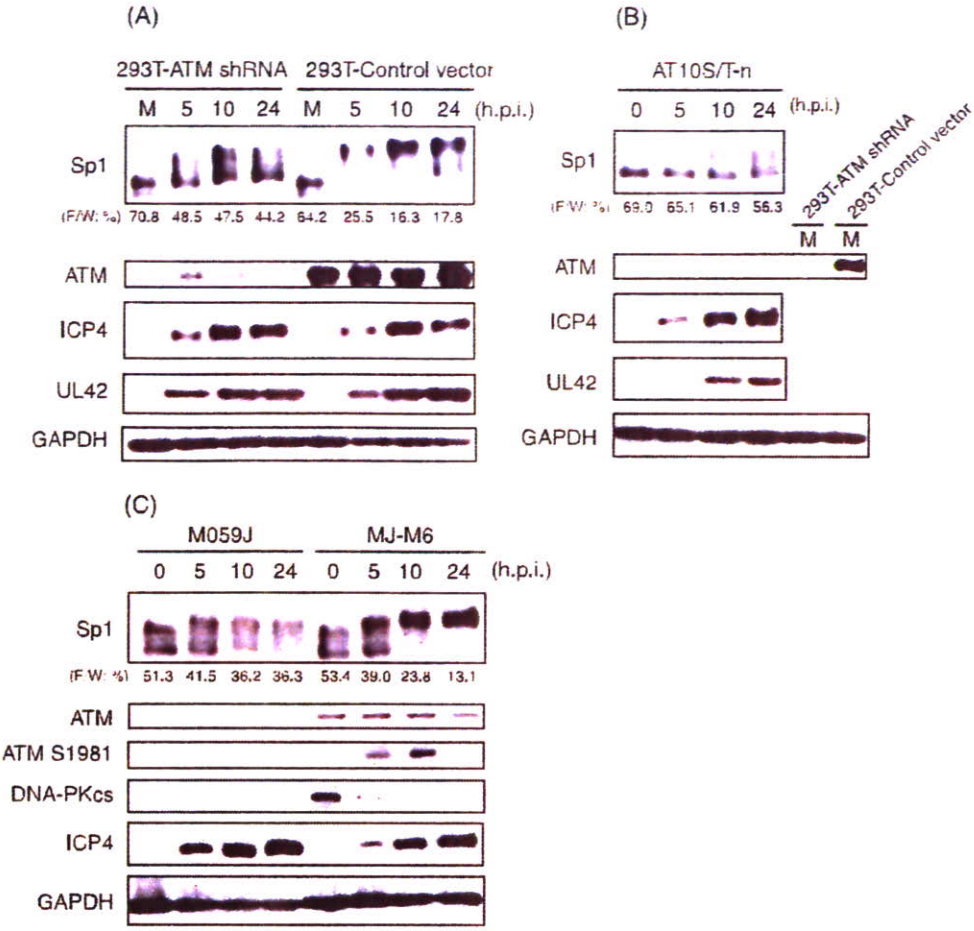

FIG. 3. ATM is involved in hyperphosphorylation of Sp1 induced by HSV-1 infection. (A and B) 293T-ATM shRNA and 293T-Control vector cells (A) and ATM defective AT10S/T-n cells (B) were infected with HSV-1 at an MOI of 10 and harvested at the indicated times postinfection. Whole-cell lysates were prepared, and equal amounts of proteins from each sample (7 to 15 μg) were subjected to immunoblot analysis with the indicated antibodies. Each value at the bottom of the panel of Sp1 ("F/W: %") represents the percentage of the level of the faster-migrating form to whole amounts of Sp1, calculated as described in Materials and Methods. M, mock infection. (C) Human glioma M059J (DNA-PKcs null and the lower level of ATM) and MJ-M6 (M059J cells expressing DNA-PKcs) cells were infected with HSV-1 at an MOI of 2.5 and harvested at the indicated times postinfection. Whole-cell lysates (15 μg) were subjected to immunoblot analysis for expression profiles of Sp1, ATM, ATM phosphorylated at Ser-1981, DNA-PKcs, ICP4, and GAPDH. Anti-GAPDH antibody was used to confirm equal protein loading.

viral ubiquitin ligase (35, 44). In contrast, in DNA-PKcs-defective M059J cells, the slower-migrating form of Sp1 appeared from 5 hpi and subsequently did not increase. Although the ATM phosphorylated at Ser-1981 increased slowly with progression of HSV-1 infection, the expression level was very low, reflecting the phosphorylation status of Sp1 in M059J cells. The expression profile of ICP4 was almost the same in both M059J and MJ-M6 cells. Overall, the results strongly suggest that activated ATM is involved directly or indirectly in the hyperphosphorylation of Sp1 in response to HSV-1 infection.

After IR, Sp1 is hyperphosphorylated dependent on activated ATM. In order to determine whether activation of ATM induces hyperphosphorylation of Sp1, HFF2 cells were exposed to 10 Gy of gamma irradiation, which generates double-strand DNA breaks, leading to activation of ATM-dependent DNA damage signal transduction. As shown in Fig. 4A, Sp1 was hyperphosphorylated immediately after IR accompanied by phosphorylation of Ser-1981 of ATM, leading to catalytic activation of the protein.

To determine whether IR-induced Sp1 phosphorylation depends on activated ATM, ATM-silenced 293T cells (293T-ATM shRNA) and 293T-Control vector cells were exposed to gamma irradiation (20 Gy) (Fig. 4B). In 293T-Control vector cells, IR induced the phosphorylation of ATM at Ser-1981 by 15 min post-IR, and simultaneously more than half of the Sp1 proteins were converted to hyperphosphorylated and slower-migrating forms. In contrast, in IR-treated ATM expression-silenced 293T cells, the phosphorylation status of Sp1 was almost unchanged. These observations with IR support the idea that the hyperphosphorylation of Sp1 is directly or indirectly dependent on activated ATM.

Mapping of Sp1 phosphorylation sites induced upon HSV-1 infection. Related PI-3-like kinases family members, ATM, DNA-PK, and ATR (ATM-Rad3-related), display kinase activity against serine (S) and threonine (T), followed by glutamine (Q) (SQ or TQ), residues (1, 6, 12, 13). Sp1 possesses 11 SQ sites and four TQ sites (Fig. 5A). With the aim of determination of the phosphorylation site(s), we constructed

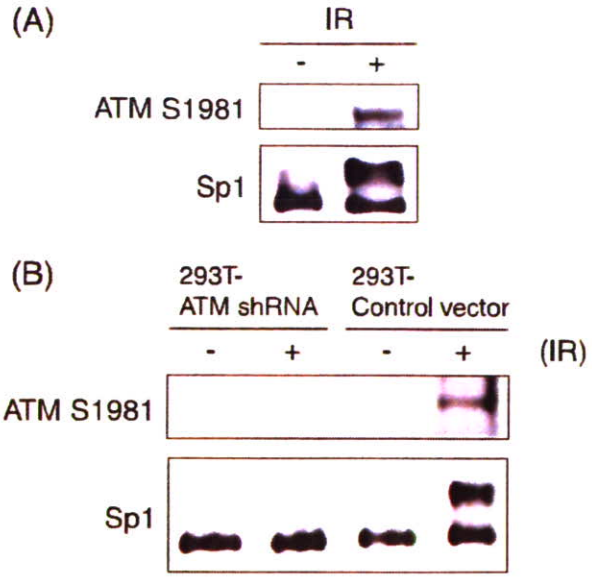

FIG. 4. (A) Hyperphosphorylation of Sp1 induced upon exposure to IR. HFF2 cells were exposed to gamma irradiation (IR) with 10 Gy and harvested at 15 min post-IR. Whole-cell lysates were prepared, and 30-μg aliquots of proteins from each sample were subjected to immunoblot analysis with anti-Sp1 and ATM S1981 antibodies. (B) Sp1 hyperphosphorylation induced upon IR is correlated with the activation of ATM. The 293T-ATM shRNA and 293T-Control vector cells were exposed to IR with 20 Gy and harvested at 15 min post-IR. Whole-cell lysates were prepared, and equal amounts of proteins from each sample were subjected to immunoblot analysis with anti-Sp1 and ATM S1981 antibodies. −, No IR.

expression vectors of Flag-tagged Sp1 (Flag-Sp1) containing alanine mutations of serine/threonine in each SQ/TQ site and investigated their phosphorylation in HSV-1-infected cells. As shown in Fig. 5B, most of the exogenously expressed Flag-tagged wild-type Sp1, like endogenous Sp1, was converted to slower-migrating forms upon HSV-1 infection, although a part of the recombinant protein (25 to 36%) remained as the faster-migrating form at 24 hpi. Phosphorylation patterns of Sp1 containing alanine mutations of Ser-36, Ser-81, Ser-85, Thr-98, Thr-250, Ser-281, Ser-291, Ser-296, Ser-313, Ser-351, Thr-394, Thr-427, and Ser-431 were almost the same as that of wild-type Sp1. The percentages of the remaining faster-migrating form to the total amounts of those mutated Sp1 were almost the same as or less than that of wild-type Sp1 (Fig. 5B, lower panel). In contrast, although Flag-Sp1 containing an alanine mutation of either Ser-56 or Ser-101 was also phosphorylated upon HSV-1 infection, the percentages of the faster-migrating form to total Sp1 were much higher (45 to 57%) compared to that seen with wild-type Sp1 (25%) (Fig. 5B, upper panel). Furthermore, Flag-Sp1 containing alanine mutations at both Ser-56 and Ser-101 resulted in considerably impaired conversion to the slower-migrating and hyperphosphorylated forms upon HSV-1 infection. Thus, mutation of Ser residues 56 and 101 individually or in tandem to alanine resulted in a reduction of the hyperphosphorylation of Sp1 upon HSV-1 infection.

Kim and DeLuca suggested that Sp1 is important for the expression of immediate-early and early genes whose promoters possess Sp1 binding sites and predicted that its hyperphosphorylation contributed to the downregulation of expression of these gene classes late in infection (31). However, the expression levels of ICP4 were almost constant among cells expressing wild-type Sp1 and a variety of mutated Sp1 proteins (Fig. 5B). Thus, even when the mutated Sp1 at Ser-56 and Ser-101 was expressed exogenously, we did not observe any reduced or overaccumulation of the immediate-early protein, ICP4, compared to exogenously expressed wild-type Sp1.

Ser-56 and Ser-101 on Sp1 become phosphorylated upon HSV-1 infection. In order to confirm that Sp1 is phosphorylated at Ser-56 and Ser-101 during HSV-1 infection, we prepared phosphopeptide-specific antibodies (α-Sp1 [pS56] and α-Sp1 [pS101] antibodies) raised against phosphorylated Ser-56 and Ser-101 residues, respectively, and characterized the specificity of each antibody (Fig. 6A and B). Exogenously expressed Sp1 proteins were immunoprecipitated with anti-Flag antibody from whole-cell lysates of HeLa cells that were transfected with each expression vector—pcDNA-RHF/Sp1, pcDNA-RHF/Sp1-S56A, or pcDNA-RHF/Sp1-S101A—followed by HSV-1 infection. Immunoprecipitated wild-type and mutant Sp1 samples were subjected to immunoblot analysis with the phosphopeptide-specific antibodies (Fig. 6A). α-Sp1 (pS56) could recognize wild-type Flag-Sp1 but not Flag-Sp1-S56A. Similarly, α-Sp1 (pS101) recognized wild-type Flag-Sp1 but not Flag-Sp1-S101A. In addition, both α-Sp1 (pS56) and α-Sp1 (pS101) showed CIAP-sensitive reactivity with endogenous Sp1 in whole-cell lysates obtained from HSV-1-infected HeLa cells at 12 hpi (Fig. 6B). Thus, it was proved that these two antibodies are directed against phospho-Ser-56 and phospho-Ser-101, respectively.

Next, we examined phosphorylation of Sp1 at Ser-56 and Ser-101 in HeLa cells and the ATM-deficient cell line, AT10S/T-n, throughout HSV-1 infection using the phosphopeptide-specific antibodies (Fig. 6C and D). In HeLa cells, phosphorylation of Sp1 at Ser-56 or Ser-101 was detected by 4 hpi and reached maximum level at 8 hpi. Similarly, the activated ATM phosphorylated at Ser-1981 was detected by 4 hpi and increased gradually. In contrast, in AT10S/T-n cells, both residues on Sp1 were not phosphorylated at all throughout infection. These observations clearly showed that both Ser-56 and Ser-101 residues on Sp1 become phosphorylated directly or indirectly by ATM in response to HSV-1 infection.

ATM phosphorylates Ser-101 but not Ser-56 on Sp1 in vitro. In order to investigate whether ATM can phosphorylate Sp1 directly, IP-kinase assays were performed (Fig. 7). Purified Sp1 from insect cells was subjected to an in vitro kinase assay with Flag-tagged wild-type ATM and kinase-dead ATM immunoprecipitated by anti-Flag antibody from cells transfected with each expression vector. Purified p53 known as a substrate for ATM (6) was used as a positive control. Equal amounts of Flag-tagged wild-type ATM and kinase-dead ATM were immunoprecipitated by anti-Flag antibodies. As shown in Fig. 7, Flag-tagged wild-type ATM phosphorylated Sp1 and p53 directly, whereas kinase-dead ATM did not. Thus, ATM can directly phosphorylate Sp1 in vitro.

Next, to determine whether ATM can phosphorylate Ser-56 and Ser-101 on Sp1 directly, GST fusion proteins of truncated Sp1 (8 to 167 amino acids) (GST-$Sp1_{8-167}$) and identical fragments with Ser-56 or Ser-101 or both mutated to alanine (GST-$Sp1_{8-167}$-S56A, GST-$Sp1_{8-167}$-S101A, and GST-$Sp1_{8-167}$-S56/101A) (Fig. 8A) were used as substrates in IP-kinase as-

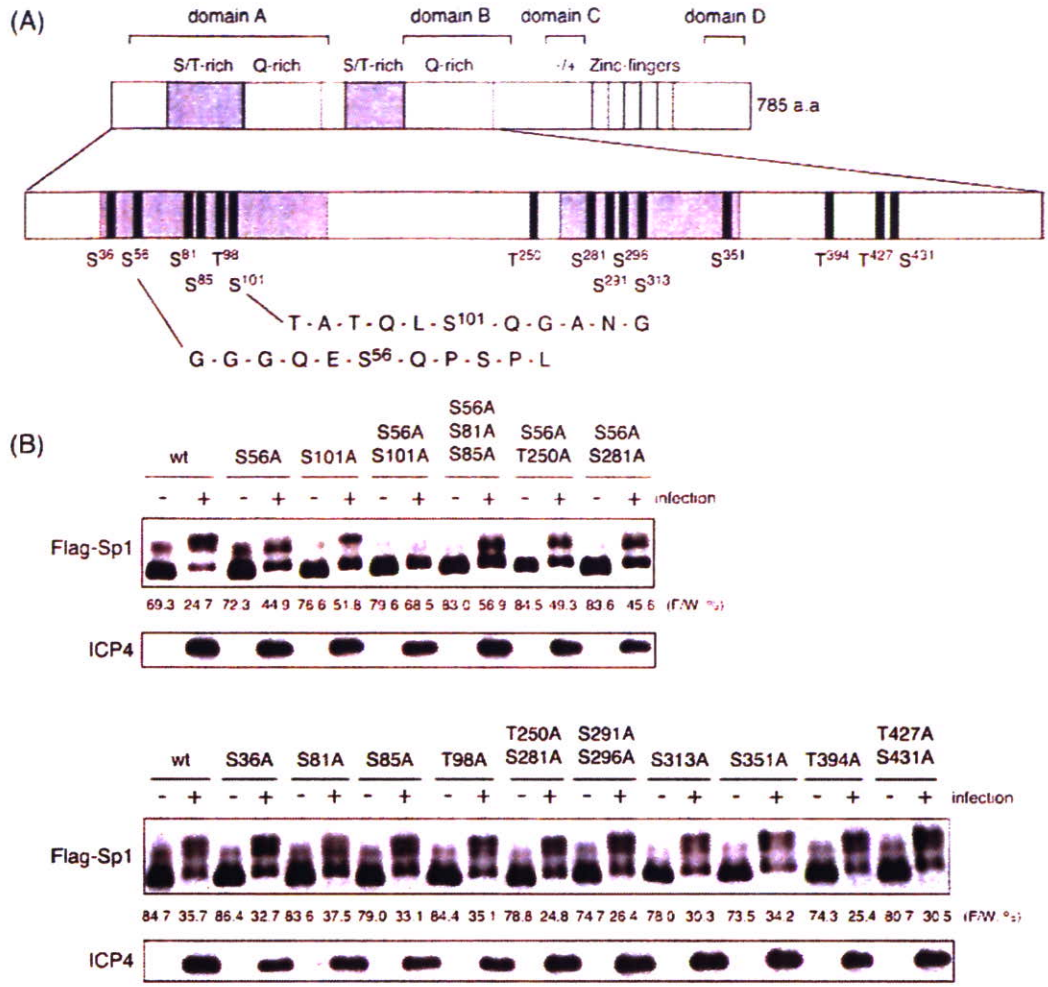

FIG. 5. Mapping of phosphorylation sites of Sp1 upon HSV-1 infection. (A) Schematic diagram of functional domains and putative ATM phosphorylation sites of Sp1. The 785 amino acids of Sp1 have two S/T-rich regions, two Q-rich regions, and three zinc fingers. The domains A, B, C, and D correspond to multiple transcriptional activation domains. The sign "−/+" represents a region of high charge density (14). Motifs of serine (S) or threonine (T), followed by glutamine (Q) (SQ and TQ) in Sp1, are putative phosphorylation sites for ATM. Sp1 contains 15 SQ and TQ sites. The amino acid sequences around Ser-56 and Ser-101 are shown in detail. (B) HeLa cells were transfected with pcDNA-RHF/Sp1 expressing wild-type (wt) Sp1 or a variety of expression vectors for mutated Sp1 containing the indicated serine or threonine residues replaced with alanine. Cells were infected with HSV-1 at an MOI of 10 at 24 h posttransfection and harvested at 24 hpi. Whole-cell lysates were prepared, and 25-μg portions of proteins from each sample were subjected to immunoblot analysis with anti-ICP4 antibody or anti-Flag antibody to detect exogenously expressed Sp1 proteins (Flag-Sp1). Each value at the bottom of the panel of Flag-Sp1 ("F/W: %") represents the percentage of level of the faster-migrating form to whole amounts of Flag-Sp1 as described in Materials and Methods.

says. The amounts of immunoprecipitated Flag-tagged wild-type ATM and kinase-dead ATM proved the same on immunoblot analysis (Fig. 8B). As shown in Fig. 8C, GST-$Sp1_{8-167}$-S56A, as well as wild-type GST-$Sp1_{8-167}$, was phosphorylated by wild-type ATM but not by kinase-dead ATM. In contrast, wild-type ATM could not phosphorylate GST-$Sp1_{8-167}$-S101A or GST-$Sp1_{8-167}$-S56/101A. These results clearly indicate that ATM can directly phosphorylate Sp1 at Ser-101 but not Ser-56. Considering this and the result that neither Ser-101 nor Ser-56 were phosphorylated upon HSV-1 infection in the ATM-defective cell line (Fig. 6D) together, other kinase(s) activated by ATM would phosphorylate Ser-56 on Sp1 upon HSV-1 infection.

ATM-dependent Sp1 phosphorylation does not affect Sp1-dependent transcriptional activity during viral infection. In order to examine whether ATM affects Sp1-dependent transcriptional activity upon HSV-1 infection, CAT activity from the Sp1 responsive promoter in ATM expression-silenced 293T cells (293T-ATM shRNA) was compared to those in ATM expression-intact 293T cells (293T-Control vector) (Fig. 9). Sp1 stimulates transcription from promoters containing a GC-rich recognition element, the GC-box (15, 16, 19), and is also important for the regulation of TATA-less genes that encode housekeeping proteins (23). As depicted in Fig. 9A, the CAT reporter plasmid, p65F1CAT, has a promoter sequence (−575 to +38) of p65, an NF-κB subunit, containing three GC-boxes upstream of the CAT gene without any TATA consensus sequence (62). 293T-ATM shRNA cells and 293T-Control vector cells transfected with p65F1CAT were infected with HSV-1 at 24 h posttransfection and harvested at 12 hpi. The lysates from

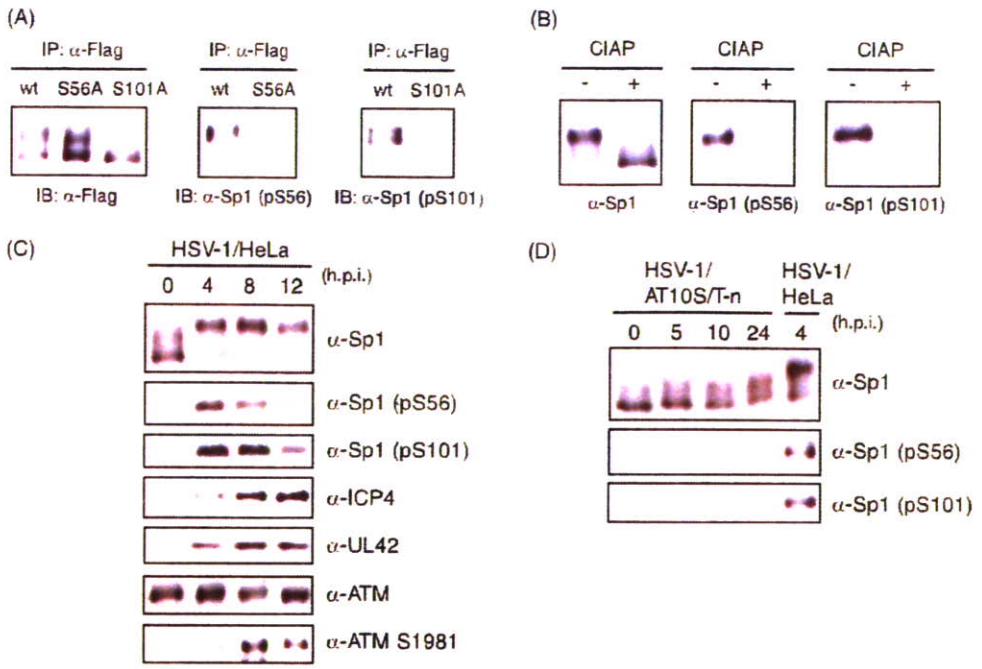

FIG. 6. Ser-56 and Ser-101 of Sp1 are phosphorylated upon HSV-1 infection. (A) HeLa cells were transfected with pcDNA-RHF/Sp1 (wt), pcDNA-RHF/Sp1-S56A, or pcDNA-RHF/Sp1-S101A and infected with HSV-1 at an MOI of 10 at 24 h posttransfection. At 24 hpi, cells were harvested and lysed. The whole-cell lysates were subjected to IP with anti-Flag M2 affinity resin, and the immunoprecipitated samples were subjected to immunoblot (IB) analysis with anti-Flag, α-Sp1 (pS56), and α-Sp1 (pS101) antibodies. (B) Whole-cell lysates obtained from HSV-1-infected HeLa cells at 12 hpi were treated with (+) or without (−) CIAP. The samples were applied for immunoblot analysis with the indicated antibodies. (C) HeLa cells were infected with HSV-1 at an MOI of 10 and harvested at the indicated times postinfection. Whole-cell lysates were prepared, and equal amounts of proteins from each sample were applied for immunoblot analysis with the indicated antibodies. (D) AT10S/T-n cells were infected with HSV-1 at an MOI of 10 and harvested at the indicated times postinfection. Whole-cell lysates were prepared and subjected to immunoblot analysis with the indicated antibodies. Whole-cell lysate from HSV-1-infected HeLa cells at 4 hpi was also applied as a positive control.

both cells were subjected to CAT assay, and the transcriptional activities were analyzed by calculating the percentage of the conversion of unacetylated [^{14}C]chloramphenicol to the acetylated form. In a CAT assay for p65F1CAT, the transcriptional activity from the Sp1 responsive promoter in 293T-ATM shRNA cells was almost the same (only a 1.2-fold increase) as that in 293T-Control vector cells (Fig. 9B and C). Next, another reporter plasmid, pCAT TATA+Sp1(−55)+Sp1(−75) (Fig. 9D) containing two GC-boxes and TATA consensus sequence of human cytomegalovirus (HMCV) major immediate-early gene upstream of the CAT gene (27) was used as TATA-dependent Sp1 responsive promoter. Similarly, the transcriptional activity from the promoter in 293T-ATM shRNA cells infected with HSV-1 was almost the same as that in 293T-Control vector cells (Fig. 9E and F). In 293T-Control vector cells Sp1 was detected mainly as the slower-migrating and hyperphosphorylated forms at 12 hpi. In contrast, in 293T-ATM shRNA cells, Sp1 was detected mostly as the faster-migrating form and partially as the slower-migrating form (Fig. 9C and F, inset images). Phosphorylation of Ser-56 and Ser-101 on Sp1 was observed in 293T-Control vector cells, while the phosphorylation was not in 293T-ATM shRNA cells (data not shown). As shown in Fig. 3A, the expression profiles of ICP4, whose promoter possesses several Sp1-binding sites, in 293T-ATM shRNA and 293T-Control vector cells were almost the same throughout HSV-1 infection, corresponding well with the same Sp1-dependent transcriptional activities in both cells obtained in the reporter-gene analyses of Fig. 9. Collectively, ATM-dependent Sp1 phosphorylation does not appear to affect the Sp1-dependent transcriptional activity during viral infection.

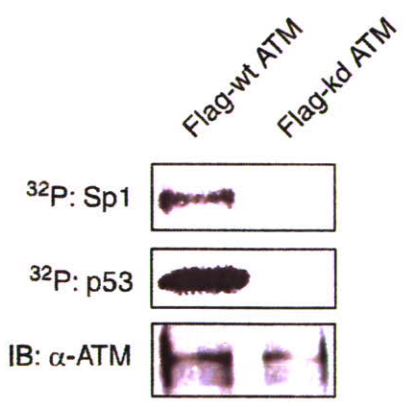

FIG. 7. Sp1 is phosphorylated by ATM in vitro. The lysates of 293T cells transfected with plasmid expressing Flag-tagged wild-type ATM (Flag-wt ATM) or kinase-dead ATM (Flag-kd ATM) were immunoprecipitated with anti-Flag antibody. Each of immunocomplexes containing Flag-wt ATM or Flag-kd ATM protein were incubated with purified Sp1 or p53 as substrates in the presence of [γ-^{32}P]ATP. Sp1 and p53 were resolved by SDS–10% PAGE, followed by autoradiography. The amounts of immunoprecipitated Flag-wt ATM and Flag-kd ATM were confirmed by immunoblot analysis with anti-ATM antibody.